UCRL-ID-151071

# Preliminary Report on the Population of the $^{235}U$ $T_{1/2}$ = 25-Minute Isomer by the (n,n$'\gamma$) Reaction

*W. Younes, H. C. Britt, J. A. Becker, L. A. Bernstein, P. E. Garrett, C. A. McGrath, D. P. McNabb, R. O. Nelson, M. Devlin, N. Fotiades*

**October 9, 2002**

U.S. Department of Energy
Lawrence Livermore National Laboratory

## DISCLAIMER



This work was performed under the auspices of the U. S. Department of Energy by the University of California, Lawrence Livermore National Laboratory under Contract No. W-7405-Eng-48.

# Preliminary Report on the Population of the $^{235}$U $T_{1/2}$ = 25-minute Isomer by the (n,n'$\gamma$) Reaction

W. Younes,* H. C. Britt, J. A. Becker, L. A. Bernstein, P. E. Garrett, C. A. McGrath,† and D. P. McNabb
*Lawrence Livermore National Laboratory, Livermore, CA 94551*

R. O. Nelson, M. Devlin, and N. Fotiades
*Los Alamos National Laboratory, Los Alamos, NM 87545*
(Dated: October 9, 2002)

The population cross section of the $T_{1/2}$ = 25-minute, $E_x$ = 76.8-keV isomer in $^{235}$U via the $^{235}$U(n,n'$\gamma$) reaction has been estimated in the $E_n$ = 2.1–20-MeV range. Gamma rays populating both isomer and ground states were detected using the GEANIE spectrometer at the LANSCE/WNR "white-source" neutron facility. Partial $\gamma$-ray cross sections were obtained as a function of incident neutron energy, using $\gamma$-ray spectroscopy and the time-of-flight technique. A correction for unobserved transitions was applied to the measured partial cross sections using the Hauser-Feshbach code GNASH to produce population cross sections for the isomer- and ground-state levels. The deduced isomer population cross section at $E_n$ = 2.1 MeV is 1.1(1) b, and the isomer-to-ground state population ratio decreases from 0.9 to 0.06 over the $E_n$ = 2.1–20-MeV range. The details of the measurement and recommendations to improve the current results are discussed.

## I. INTRODUCTION

Measurements [1–3] of the neutron-induced fission cross-section for the $E_x$ = 76.8-eV, 25-minute, isomer in $^{235}$U have shown a marked enhancement over the fission cross section induced on the ground state near thermal- and cold-neutron energies, corresponding to a neutron-energy range from a few to tens of meV. Measurements of the $^{235m}$U neutron-induced fission cross section have relied on the population of the isomer by the $\alpha$ decay of the $^{239}$Pu ground state to produce a $^{235m}$U sample. At $E_n$ = 56 meV, for example, the measured [3] isomer-to-ground fission cross-section ratio of 2.47±0.45 is taken as evidence that the path to fission for the $^{235m}$U(n,f) reaction is enhanced as it proceeds through $0^+$ and $1^+$ resonance states, in analogy with neutron-induced fission of the $^{239}$Pu ground state [1]. The role of the isomer state in neutron-induced fission of $^{235}$U is of some importance in "hot" environments where, along with the Nuclear Excitation by Electron Transfer (NEET) process [4, 5], inelastic neutron interactions represent an important population mechanism for this level. Studies of the $^{235m}$U(n,f) process also have direct bearing on neutron-induced fission on the $^{239}$Pu ground state, because the $^{235m}$U and $^{239}$Pu levels have similar nuclear structure (both share the same 1/2[631] Nilsson-model configuration).

In this paper, the $^{235}$U(n,n')$^{235m}$U population cross section for $E_n$ = 1–20 MeV is deduced from partial transition cross section "feeding" the isomer, measured using the GEANIE spectrometer at the LANSCE/WNR "white-source" neutron facility, and corrected for unobserved transitions using the Hauser-Feshbach code GNASH [6]. The experimental setup is discussed briefly in section II, the GNASH calculations are described in section III, and the analysis and discussion of the $\gamma$-ray data can be found in section IV. The reader interested in the final results can consult table III and Fig. 20 for the absolute isomer-state population cross section, table IV and Fig. 21 for the absolute ground-state population cross section, and table VII and Fig. 24 for the isomer-to-ground-state population ratio.

## II. EXPERIMENTAL DETAILS

Detailed descriptions of the experimental setup can be found in references [7–9]. In particular the experimental configuration is similar to the one described in reference [9] for the data set labeled "**99Thin**". The same 0.4820(27) g/cm$^2$, 93.2%-isotopically enriched $^{235}$U sample was used and housed in the same Pu-blank container as in the **99Thin** run. In contrast to the previous experiment, however, the thin $^{nat}$Fe foils used for cross-section calibration were not included. Because of the similarity in configurations between the current and **99Thin** experiments, the spectrometer's $\gamma$-ray efficiency is expected to be the same, to a good approximation. The white neutron spectrum at

*Electronic address: younes@llnl.gov
†present address: Idaho National Engineering and Environmental Lab, Idaho Falls, ID 83415

the LANSCE/WNR facility is produced by proton-induced spallation of a $^{nat}$W target, situated 20.34 m upstream from the GEANIE spectrometer. The present data were acquired over 7.5 days of beamtime in August 2000 with a beam-micropulse spacing of 3.6 $\mu$s. Previous studies of the n+$^{235}$U reaction using the GEANIE spectrometer were carried out with a 1.8-$\mu$s micropulse spacing [9, 10]. The longer micropulse spacing in the present data eliminates contamination arising from beam "wrap-around", which occurs when slower neutrons from a previous micropulse reach the $^{235}$U sample at the same time as neutrons from the prompt (current) micropulse. The micropulses were "bunched" into 625-$\mu$s-long macropulses, repeated at a 100-Hz rate, giving an overall 6% duty cycle. The proton-beam current was 2.5 $\mu$A. Deadtimes of 71.2% and 65.7% were measured for the combined planar detectors and for the $^{235}$U-foil neutron-flux monitor, respectively.

## III. MODEL CALCULATIONS

The Hauser-Feshbach statistical code GNASH [6] has been used to calculate partial transition cross sections for the $^{235}$U(n,n') reaction. The specific calculation used in this paper is labeled "**GNASH98**" [11] and provides partial transition cross sections for decays from levels with $E_x \leq 720.2$ keV in the $E_n$ = 2.1–20-MeV range. These calculations were subsequently modified to take into account Internal-Conversion Coefficients (ICC), obtained from the ENSDF database [12], in branching-ratio values[15]. This adjustment is especially important in calculations of the $^{235}$U(n,n'$\gamma$) channel, where low-energy, highly-converted $\gamma$-ray branches often compete with higher-energy decays from the same parent level. The effect on individual partial cross sections can be seen in the relative change in the calculation listed in table I.

If several non-coincident transitions contributing to the population of a given level (denoted by $f$) can be measured, the "parallel-path" sum of their cross sections (denoted by $\sum_i \sigma_{i\rightarrow f}^{(\mathrm{meas})}$) provides a lower bound on the total population cross section for that level. Note that these individual transitions need not feed the state $f$ directly, as long as their full transition strength reaches the final state $f$. The sum over the same transitions can be carried out in the **GNASH98** calculation to produce the quantity $\sum_i \sigma_{i\rightarrow f}^{(\mathrm{GNASH98})}$, and the sum of cross sections for all non-coincident transitions directly feeding state $f$ yields the total population cross section $\sigma_f^{(\mathrm{GNASH98})}$ for that level in the calculation. The calculated partial-to-total ratio

$$\rho_f \equiv \frac{\sum_i \sigma_{i\rightarrow f}^{(\mathrm{GNASH98})}}{\sigma_f^{(\mathrm{GNASH98})}}, \tag{1}$$

is an estimate of the fraction of the total population cross section measured in the GEANIE data. The total population cross section is then deduced from the measured parallel-path sum according to

$$\sigma_f \equiv \frac{\sum_i \sigma_{i\rightarrow f}^{(\mathrm{meas})}}{\rho_f}. \tag{2}$$

This technique takes advantage of the fact that the partial-to-total ratio can be calculated more accurately by GNASH than either the partial or total-population cross sections alone. At present, no model uncertainties are available for the partial-to-total ratios calculated using GNASH, therefore only statistical uncertainties resulting from the measurement are quoted in this paper.

## IV. DISCUSSION

### A. Analysis of Individual $\gamma$ Rays

The analysis of the present data follows the procedure outlined for the analysis of the **99Thin** data set in reference [9]. Thus, $\gamma$-ray spectra corresponding to 15-ns time-of-flight (TOF) steps in the $E_n$ = 1–20 MeV range have been fitted over the $E_\gamma$ = 85–1020-keV range using the code XGAM [13]. In principle, the excitation functions could be extended further down to $E_n$ = 145 keV, with the main limitation imposed by statistics in the fission-chamber data. A total of 16 $\gamma$ rays attributed to the $^{235}$U(n,n'$\gamma$) channel are discussed in this paper. These transitions are listed in table I and placed in the $^{235}$U level scheme in Fig. 1.

The $\gamma$-ray efficiency of the GEANIE spectrometer is expected to be similar, for the present data, to the efficiency adopted in the analysis of the **99Thin** data set. In order to verify this assumption, the scale factors between $\gamma$-ray cross sections determined from the present and **99Thin** data have been calculated for a set of transitions and

neutron-energy ranges where beam wrap-around is not a concern (e.g. transitions in the $^{235}$U(n,2n$\gamma$) channel, and transitions from higher-$E_x$ states in the $^{235}$U(n,n'$\gamma$) channel). These scale factors are plotted in Fig. 2 and lie close to 1 for 100 keV $\lesssim E_\gamma \lesssim$ 300 keV, in agreement with the assumption of similar efficiencies between the two experiments. For $E_\gamma$ < 100 keV and $E_\gamma$ > 300 keV, the scale factors deviate significantly from 1. This may suggest that $\sim$ 20% adjustments to the **99Thin** efficiency could be required for the present data, but it is more likely an indication of the difficulty in fitting the especially weak $\gamma$ rays used in this case, and increased statistics as wells as an improved modeling of the neutron bumps are necessary. The $\lesssim$ 10% scale factors in the $E_\gamma$ 100–300 keV range are probably a better gauge of the size of expected adjustments to the efficiency curve.

No correction for $\gamma$-ray angular-distribution effects has been included in the present analysis, because such effects are expected to be small in the neutron-energy range of interest (i.e. $E_n$ = 2.1–20 MeV). However, if the analysis of these data is extended to lower neutron energies, such corrections will have to be taken into account.

Partial cross sections for the $^{235}$U(n,n'$\gamma$) transitions listed in table I are plotted as a function of incident neutron energy in Figs. 3-18. The corresponding calculated partial cross section is also shown, where available. The match between measured and calculated excitation functions varies in quality. In general, the agreement between theory and experiment is best for those transitions which contribute to the population of the isomer state, rather than to the ground state. A brief discussion of the data and calculations is given for individual $\gamma$ rays:

**$E_\gamma$ = 129.3 keV (Fig. 3):** the **GNASH98** calculation significantly under-predicts the GEANIE data in this case. Furthermore, even if the calculations are scaled up to ensure a match with data at $E_n$ = 2.1 MeV, a discrepancy between the two remains at higher neutron energies. This discrepancy could indicate an inadequate treatment of the pre-equilibrium channel.

**$E_\gamma$ = 160.2 keV (Fig. 4):** this transition is clearly contaminated above $E_n$ = 12 MeV by an $E_\gamma$ = 159.4(1)-keV $\gamma$-ray in the $^{235}$U(n,3n)$^{233}$U channel. Therefore, for the purposes of this paper, the partial cross section for this $\gamma$ ray has been set to zero for neutron energies above the (n,3n) reaction threshold (i.e. $E_n$ = 12.194 MeV) in both the data and the calculations, so that the contaminated data do not contribute to the estimate of the total population of the isomer level. Data and **GNASH98** predictions are in very good agreement in the range $E_n$ = 6.5-12.2 MeV, while in the $E_n$ = 2.1-6.5-MeV range, the calculation over-predicts the observed yields.

**$E_\gamma$ = 167.8 keV (Fig. 5):** the statistics for this line are poor, nevertheless GNASH over-predicts the yields by up to a factor of 3.

**$E_\gamma$ = 316.4 keV (Fig. 6):** the agreement between experiment and theory is poor in this case, especially for $E_n \geq$ 10 MeV, where the **GNASH98** cross section essentially disappears.

**$E_\gamma$ = 375.0 keV (Fig. 7):** the **GNASH98** calculation severely under-predicts the data in this case. This is the only sizeable mismatch between experiment and theory for transitions which contribute to the population of the isomer state.

**$E_\gamma$ = 380.2 keV (Fig. 8):** statistics are poor for this $\gamma$-ray, but the agreement with **GNASH98** predictions is good, albeit within large errors.

**$E_\gamma$ = 392.6/393.1 keV (Fig. 9):** the two $\gamma$-ray energies cannot be resolved in the GEANIE data. Fortunately, both transitions feed the band built on the isomer state, and are not coincident with each other. Therefore, their combined yields, measured by the GEANIE spectrometer, can be used in the evaluation of the isomer-level population. The agreement with the calculated sum of the two transition cross sections is good.

**$E_\gamma$ = 406.9 keV (Fig. 10):** there are indications in the excitation-function data of a rise starting near $E_n$ = 10 MeV, suggesting contamination by a $^{235}$U(n,3n$\gamma$) transition. However, no $\gamma$ ray with similar energy could be identified in the known level scheme of $^{233}$U. The agreement between data and **GNASH98** prediction is poor.

**$E_\gamma$ = 413.7 keV (Fig. 11):** the excitation function for this line is well reproduced by the **GNASH98** calculation . Both this and the $E_\gamma$ = 375.0-keV transition are issued from the same $E_x$ = 426.7-keV level, and both are expected to have comparable yields, based on measured branching ratios [12]. however the measured partial cross sections for these $\gamma$ rays differ by a factor of $\approx$ 3.3. Two possible explanations present themselves: either the 375.0-keV $\gamma$ ray is contaminated, or the inconsistency is due to low statistics resulting in a poor fit of the weak 413.7-keV peak. Improved statistics should help confirm or rule out the latter possibility.

**$E_\gamma$ = 445.7 keV (Fig. 12):** the excitation function for this $\gamma$ ray suffers from poor statistics. Nevertheless, the agreement with the **GNASH98** prediction is fair, within large uncertainties.

Fitted $\gamma$ rays in the $E_\gamma$ = 590–640-keV range suffer from an additional problem. The corresponding peaks in the $\gamma$-ray spectrum lie on top of a large "neutron bump" produced by the $^{74}$Ge(n,n'$\gamma$) reaction in the detectors. The resulting $E_\gamma$ = 595.8-keV, $2_1^+ \rightarrow 0_1^+$ transition can occur while the $^{74}$Ge are recoiling, thereby producing a broad feature in the spectrum, which is difficult to fit consistently as a function of varying neutron energy. The excitation function for this neutron bump is plotted in Fig. 19 and shows a localized feature near $E_n$ = 2.7 MeV, which is likely due to a poor fit near that neutron energy. The same feature can be observed in the excitation functions of all $^{235}$U(n,n'$\gamma$) lines discussed in this paper. A more sophisticated model of the neutron bump, and improved statistics for the peaks found on top of the bump will be required to eliminate this problem. For the current discussion, yields for the affected $^{235}$U(n,n'$\gamma$) transitions in the $E_n$ = 2-4-MeV range have been omitted as a precaution in both experiment and GNASH calculations when evaluating the summed contributions of partial $\gamma$-ray cross sections. Notwithstanding this artifact in the data, the $\gamma$ rays with $E_\gamma > 600$ keV are discussed below:

**$E_\gamma$ = 606.9 keV (Fig. 13):** this transition from a level at $E_x$ = 777.6 keV was not included in the **GNASH98** calculations because of a discrete-level cutoff at $E_x$ = 720.2 keV. However, this $\gamma$ ray could be used to improve future GNASH calculations.

**$E_\gamma$ = 617.1/618.3 keV (Fig. 14):** a single, $E_\gamma$ = 617.9-keV transition was measured which likely represents the combination of both these transitions. Fortunately, both transitions feed the band built on the ground state, but are not coincident with each other. Therefore the sum of their yields can be used to deduce the population of the $^{235}$U ground state. The measured excitation function becomes erratic for $E_n \geq 10$ MeV, and would benefit from improved statistics.

**$E_\gamma$ = 624.8/624.8 keV (Fig. 15):** the two transitions are not resolved in the GEANIE data, but, as in the case of the 392.6/393.1-keV and 617.1/618.3-keV pairs of $\gamma$ rays, are not coincident. In this case, however, one transition feeds the isomer-state band while the other feeds the ground-state band. Therefore, this transition is best used in the extraction of the total (i.e. isomer+ground-state) population. The agreement between GEANIE data and the sum of **GNASH98** yields for the two transitions is poor.

**$E_\gamma$ = 633.1 keV (Fig. 16):** the agreement between experiment and theory in this case is fair to good.

**$E_\gamma$ = 637.7/637.8 keV (Fig. 17):** the same $E_x$ = 637.8-keV level decays to both isomer and ground states. The corresponding $\gamma$-ray energies cannot be resolved within GEANIE-detector resolution. Furthermore, the branching ratio between the two decays is not well known, therefore yields from this line can only be used to deduce the total (i.e. isomer+ground-state) population cross section, which does not require that the branching ratio be known.

**$E_\gamma$ = 674.0/674.5 keV (Fig. 18):** the observed $\gamma$ ray includes contributions from the transition issued from the $E_x$ = 720.2-keV level and from an $E_\gamma$ = 674.5-keV branch from the $E_x$ = 777.6-keV level. The measured partial cross section does not agree with the GNASH prediction.

With improvements to the model calculations, and increased statistics in the data, additional transitions in the (n,n') channel could be added to the list of currently observed $\gamma$ rays. The highest-cross-section lines (as predicted by **GNASH98**) are shown in table II, along with an assessment of the prospects for their observation in current or future GEANIE data. For most of these $\gamma$ rays, severe contamination, internal conversion, or attenuation in the sample makes their observation unlikely, even with arbitrarily large statistics. In a few cases, however, significant transitions might be extracted:

**$E_\gamma$ = 116.2 keV:** this $\gamma$ ray, which feeds the isomer band, could not be observed in the current data, due to its proximity to the U $KO_{2,3}$ x ray. It is conceivable that with significantly higher statistics and a very careful modeling of the x-ray peak shapes, the $E_\gamma$ = 116.2-keV peak could be extracted, however an alternative approach may produce this line without any additional data. The $E_\gamma$ = 116.2-keV transition is issued from the $E_x$ = 129.3-keV level, for which the $E_\gamma$ = 129.3-keV branch is observed in the present data, with excellent statistics. At present, the **GNASH98** calculations fail to adequately reproduce this transition, so that the known branching ratio cannot be used to extract the $E_\gamma$ = 116.2-keV excitation function from that of the $E_\gamma$ = 129.3-keV transition with the same reliability in both experiment and theory.

**$E_\gamma$ = 124.5 keV:** this transition is observed in the present data, but with very poor statistics (e.g. 30% uncertainties at $E_n$ = 5.6 MeV, and large fluctuations throughout its excitation-function shape). If it could be adequately measured, the known branching ratio could be used to deduce the excitation function for the strong 67.7-keV yrast transition, issued from the same parent level at $E_x$ = 170.7 keV, and feeding the ground state.

**$E_\gamma$ = 189.5 keV:** similarly, this transition is issued from a level populated with a large cross section in the **GNASH98** calculation. It could not be extracted from the present data, because the corresponding peak lies in the high-energy tail region of the strongest line in the $\gamma$-ray spectrum: an $E_\gamma$ = 185.7-keV transition in $^{231}$Th. Improved statistics and a very careful modeling of the high-energy tails in the peak shapes are required to obtain the excitation function for the $E_\gamma$ = 189.5-keV transition. Furthermore, the parent level, with $E_x$ = 438.6 keV, is modeled in the **GNASH98** calculation as having two $\gamma$-ray branches: the weak 189.5-keV decay, and a strong 100.0-keV decay. However, the ENSDF [12] database shows only one transition from this level. Therefore, further evaluation of other experimental work on this level may be required before the 189.5-keV transition can be properly modeled.

### B. Absolute Population Cross Sections

The individual $\gamma$-ray excitation functions were added to form partial sums of transition cross sections feeding either the isomer or ground state, and combined with the corresponding **GNASH98** prediction to extract population cross sections for these levels. In practice, because some transitions which decayed to the isomer band could not be resolved from $\gamma$ rays which fed the ground state (this is specifically the case for the $E_\gamma$ = 625-keV and 638-keV transitions discussed in the previous section), separate analyses have been performed to extract the population cross section of i) the isomer level alone, ii) the ground state alone, and iii) both isomer and ground states. The set of $\gamma$ rays that were included in the corresponding three sums of partial cross sections are identified in table I.

The analysis procedure used to extract the population cross section for the isomer level is summarized in table III and Fig. 20. Panel a) compares the partial sums from both experiment and theory, and the inset shows the partial-to-total ratio from theory, used to extract the total population of the isomer state. The deduced population cross section for the isomer level is shown in panel b), where it is compared to the corresponding **GNASH98** prediction. It should be noted that the GEANIE data show a rise in the partial-sum excitation function as $E_n$ decreases below 2 MeV (Fig. 20a). This rise is observed for individual transitions from band built on the the $E_x$ = 393.2-keV state, but not in the $E_\gamma$ = 160.2-keV isomer-band transition. The extension of GNASH calculations to lower incident-neutron energies will help determine whether this effect is an expected consequence of the feeding pattern of the levels involved. The calculated partial-to-total ratio shown in the inset to panel a) suffers from oscillations in the $E_n$ = 18-20 MeV range. This behavior is present in the GNASH calculations, but produces a negligible perturbation to the value of the ratio. It was noted in discussions above that excitation functions from individual transitions contributing to the population of the isomer level are, for the most part, in good agreement with the **GNASH98** prediction. Therefore, it is not surprising that the population of the isomer level, deduced from the combination of GNASH calculations and GEANIE data, is also well reproduced.

A similar analysis has been carried out to extract the prompt population of the ground state of the $^{235}$U nucleus. This analysis is summarized in table IV and Fig. 21. Discontinuities in the data at $E_n$ = 2 and 4 MeV in Fig. 21b) follow from the omission of yields from 590 keV < $E_\gamma$ < 640 keV transitions in the $E_n$ = 2-4-MeV range. These yields were excluded because of problems in the $\gamma$-ray fits discussed above. For the sake of consistency, the corresponding yields were also excluded from the **GNASH98** calculation. Unlike the extracted population of the isomer level, the deduced ground-state population of the nucleus does not agree with the **GNASH98** prediction.

The analysis of the total population of the $^{235}$U nucleus (i.e. isomer + ground state) is summarized in table V and Fig. 22. A small kink near $E_n$ = 7 MeV can be seen in the calculated partial-to-total ratio, shown in the inset to panel a). This effect is an artifact of the division, but is negligible for all practical purposes. The same discontinuity in the data at $E_n$ = 2 and 4 MeV seen in panel a) is due to the omission of yields from $E_\gamma$ > 600-keV transitions in the $E_n$ = 2-4-MeV range, as in the case of the ground-state population analysis (see Fig. 21b) for comparison). The deduced total population of the nucleus does not agree with the **GNASH98** prediction.

### C. Isomer-to-Ground-State Population Ratio

The isomer-to-ground population ratio $\sigma_m/\sigma_g$ has been calculated by two slightly different methods: i) using the extracted isomer-state and total population cross sections, and ii) using the extracted isomer- and ground-state population cross sections. The ratio obtained using the isomer-state and total population cross sections is based on the numbers given in tables III and V. The formula for the ratio described in appendix A is used, because it is free from correlated uncertainties. The ratio $\sigma_m/\sigma_g$ obtained using this method is plotted in Fig. 23. Alternatively, $\sigma_m/\sigma_g$ can be calculated directly from the isomer- and ground-state population cross sections, given in tables III and IV, respectively. The corresponding ratio is plotted in Fig. 24.

In principle, the values of $\sigma_m/\sigma_g$ calculated using the extracted isomer-state and total population cross sections should be more reliable than the alternative technique, because they include contributions from additional $\gamma$ rays ($E_\gamma$ = 625 keV and 638 keV). In the present data set however, these additional transitions carry large uncertainties and the second approach (table VII Fig. 24), which relies directly on the ratio between isomer- and ground-state population cross sections is preferred.

## V. CONCLUSION AND RECOMMENDATIONS

The isomer population cross section has been deduced from partial $\gamma$-ray cross sections measured with GEANIE, and the partial-to-total ratios calculated using the code GNASH. The overall isomer population, deduced from individual transitions which contribute to the population of the isomer, is in good agreement with GNASH predictions. A similar approach used to extract the population of the ground state from the GEANIE produces a significant discrepancy with the GNASH prediction. Improved statistics and further data analysis are necessary, but even so, it is unlikely that more than $\sim$ 30% of all the decay strength populating the isomer level can ever be observed using $\gamma$-ray spectroscopy alone. Therefore, it is imperative that the model calculations, used to compensate for unobserved transitions, be made as reliable as possible, using the GEANIE data as a constraint.

In order to improve the results discussed in this paper, the following recommendations are made:

- Continue analysis of current data:
  - extend excitation functions down to $E_n$ = 145 keV
  - include angular-distribution correction for lower neutron energies
  - extract proper efficiency correction factors
- Supplement with additional data:
  - improve statistics in currently observed lines
  - improve fit of lines located on top of the neutron bump in the $E_\gamma$ = 590-640-keV range
  - identify and resolve $\gamma$-ray contamination issues by comparing branches from the same level
  - extract weaker branches from strongly-populated levels, using branching ratios to recover unobserved transitions
- Improve model calculations:
  - improve overall cross-section magnitude for transitions which contribute to the population of the ground state
  - improve treatment of pre-equilibrium-reaction contribution
  - extend current calculations down to $E_n$ = 145 keV
  - update current level-scheme input file for GNASH: include additional levels above $E_x$ = 720.2 keV and correct branching ratios

## VI. ACKNOWLEDGMENTS

This work was performed under the auspices of the U.S. Department of Energy by the University of California, Lawrence Livermore National Laboratory under contract No. W-7405-Eng-48. This work has benefited from the use of the Los Alamos Neutron Science Center at Los Alamos National Laboratory. This facility is funded by the US Department of Energy under contract W-7405-ENG-36.

---

[1] V. I. Mostovoi and G. I. Ustroiev, Atomnaya Energiia **57**, 241 (1984).
[2] W. L. Talbert, J. W. Starner, R. J. Estep, S. J. Balestrini, M. Attrep, D. W. Efurd, and F. R. Roensch, Physical Review **C 36**, 1896 (1987).
[3] A. D'Eer, C. Wagemans, M. N. de Mévergnies, F. Gönnenwein, P. Geltenbort, M. S. Moore, and J. Pauwels, Physical Review **C 38**, 1270 (1988).

[4] M. R. Harston and J. F. Chemin, Phys. Rev. C **59**(5), 2462 (1999).
[5] J. B. Wilhelmy (2001), private communication.
[6] P. G. Young, E. D. Arthur, and M. B. Chadwick, *Comprehensive Nuclear Model Calculations: Introduction to the Theory and Use of the GNASH Code*, Tech. Rep. LA-12343-MS, LANL (1992).
[7] P. W. Lisowski, C. D. Bowman, G. J. Russell, and S. A. Wender, Nuclear Science and Engineering **106**, 208 (1990).
[8] J. A. Becker and R. O. Nelson, Nuclear Physics News International **7**, 11 (1997).
[9] W. Younes, J. A. Becker, L. A. Bernstein, P. E. Garrett, C. A. McGrath, D. P. McNabb, R. O. Nelson, M. Devlin, N. Fotiades, and G. D. Johns, *The 235U(n,2nγ) Yrast Partial Gamma-Ray Cross Sections: A Report on the 1998 and 1999 GEANIE Data and Analysis Techniques*, Tech. Rep. UCRL-ID-140313, LLNL (2000).
[10] W. Younes, J. A. Becker, L. A. Bernstein, D. E. Archer, M. A. Stoyer, D. P. McNabb, K. Hauschild, D. M. Drake, G. D. Johns, R. O. Nelson, and W. S. Wilburn, *Measurement of the 235U(n,2n) Cross Section using GEANIE at LANSCE/WNR: Progress Report on the 1997 Data and Analysis Techniques*, Tech. Rep. UCRL-ID-132627, LLNL (1998).
[11] M. B. Chadwick (2000), private communication.
[12] Data extracted using the NNDC On-Line Data Service from the ENSDF database, file revised as of 7/17/00. M.R. Bhat, *Evaluated Nuclear Structure Data File (ENSDF)*, **Nuclear Data for Science and Technology**, page 817, edited by S.M. Qaim (springer-Verlag, Berlin, Germany, 1992).
[13] W. Younes, *The XGAM Peak-Fitting Code*, Tech. Rep., LLNL (2003), manuscript in preparation.
[14] P. R. Bevington and D. K. Robinson, *Data Reduction and Error Analysis for the Physical Sciences* (McGraw-Hill, San Francisco, 1992), 2nd ed.
[15] in practice, the code **readgnash.v2** was written to regenerate the γ-ray cascade with ICC-corrected branching ratios, based on the **GNASH98** partial cross section, calculated with the uncorrected branching ratios.

## APPENDIX A: ERROR PROPAGATION FOR THE POPULATION RATIO

The individual partial γ-ray cross sections, measured in the present GEANIE data set can be combined into three distinct sums:

$\sum_i \sigma_{i\to g}^{(\mathrm{meas})}$: the sum of measured partial cross sections taken over non-coincident paths which promptly feed the ground state alone,

$\sum_i \sigma_{i\to m}^{(\mathrm{meas})}$: the sum of measured partial cross sections taken over non-coincident paths which promptly feed the isomer state alone,

$\sum_i \sigma_{i\to g\&m}^{(\mathrm{meas})}$: the sum of measured partial cross sections taken over non-coincident paths which promptly feed both the isomer and the ground state, but cannot be resolved in the experimental data.

By definition, these three sums do not share any common terms, and the measured total population cross section, given in table V, is simply:

$$\sum_i \sigma_{i\to g+m}^{(\mathrm{meas})} \equiv \sum_i \sigma_{i\to g}^{(\mathrm{meas})} + \sum_i \sigma_{i\to m}^{(\mathrm{meas})} + \sum_i \sigma_{i\to g\&m}^{(\mathrm{meas})} \tag{A1}$$

The **GNASH98** calculations provide a partial-to-total ratio $\rho$ for each of these measured sums over parallel paths. In particular:

$$\rho_g \equiv \frac{\sum_i \sigma_{i\to g}^{(\mathrm{GNASH98})}}{\sigma_g^{(\mathrm{GNASH98})}} \tag{A2}$$

$$\rho_m \equiv \frac{\sum_i \sigma_{i\to m}^{(\mathrm{GNASH98})}}{\sigma_m^{(\mathrm{GNASH98})}} \tag{A3}$$

$$\rho_{g+m} \equiv \frac{\sum_i \sigma_{i\to g+m}^{(\mathrm{GNASH98})}}{\sigma_{g+m}^{(\mathrm{GNASH98})}} \tag{A4}$$

where the summation is carried out in each case over the same transitions as in the corresponding measured sum. The cross sections $\sigma_g^{(\mathrm{GNASH98})}$, $\sigma_m^{(\mathrm{GNASH98})}$, and $\sigma_{g+m}^{(\mathrm{GNASH98})}$ represent the population cross sections for the ground state, isomeric state, and for their combined population, respectively, as predicted by GNASH. The isomer-to-ground-state population ratio can be calculated from the total ($\sigma_{g+m}$) and ground-state ($\sigma_g$) populations as:

$$\frac{\sigma_m}{\sigma_g} = \frac{\sigma_{g+m} - \sigma_g}{\sigma_g} = \frac{\frac{\sum_i \sigma_{i\rightarrow g+m}^{(\mathrm{meas})}}{\rho_{g+m}}}{\frac{\sum_i \sigma_{i\rightarrow g}^{(\mathrm{meas})}}{\rho_g}} - 1 \tag{A5}$$

Although Eq. A5 is strictly correct, the measured sums in the numerator and denominator share many common terms, and their uncertainties are therefore correlated. These correlations can be explicitly eliminated by substituting Eq. A1 into Eq. A5. After some straightforward algebra, this yields:

$$\frac{\sigma_m}{\sigma_g} = \frac{\rho_g}{\rho_{g+m}} \left( 1 + \frac{\sum_i \sigma_{i\rightarrow m}^{(\mathrm{meas})} + \sum_i \sigma_{i\rightarrow g\&m}^{(\mathrm{meas})}}{\sum_i \sigma_{i\rightarrow g}^{(\mathrm{meas})}} \right) - 1 \tag{A6}$$

The measured sums in this expression have no terms in common, and the uncertainty in the isomer-to-ground-state population ratio can be readily calculated [14].

Alternatively, The isomer-to-ground-state population ratio can also be calculated directly from the isomer- and ground-state population cross sections:

$$\frac{\sigma_m}{\sigma_g} = \frac{\frac{\sum_i \sigma_{i\rightarrow m}^{(\mathrm{meas})}}{\rho_m}}{\frac{\sum_i \sigma_{i\rightarrow g}^{(\mathrm{meas})}}{\rho_g}} \tag{A7}$$

In this case, the measured sums have no terms in common, and the corresponding uncertainty in the population ratio can be calculated in a straightforward manner (see, e.g., [14]).

TABLE I: Properties of $\gamma$ rays discussed in this report. The first 5 column list experimental properties, with the superscript "(meas)" indicating results measured in the current data and "(acc)" reserved for accepted ENSDF [12] values. The sixth column lists the average relative adjustment to the **GNASH98** prediction ($\Delta\sigma_\gamma/\sigma_\gamma$), after internal conversion is taken into account in the branching ratios. The seventh column shows the maximum cross section ($\sigma_\gamma^{(max)}$) attained by each transition in the **GNASH98** calculation. The last three columns show the transitions included in the sum-of-parallel-paths for the isomer-state, ground-state, and total population cross sections, respectively.

| $E_\gamma^{(meas)}$ (keV) | $E_\gamma^{(acc)}$ (keV) | $E_x$ (keV) | $\epsilon_\gamma$ | $\alpha$ | $\frac{\Delta\sigma_\gamma}{\sigma_\gamma}$ (%) | $\sigma_\gamma^{(max)}$ (b) | $\sum_i \sigma_{i\to m}^{(meas)}$ | $\sum_i \sigma_{i\to g}^{(meas)}$ | $\sum_i \sigma_{i\to g+m}^{(meas)}$ |
|---|---|---|---|---|---|---|---|---|---|
| 129.311(4) | 129.297(2) | 129.3 | 0.010770 | 0.279 | -22.4 | 0.0879 | | √ | √ |
| 160.179(48) | 160.19(5) | 357.3 | 0.013639 | 1.807 | 0.0 | 0.0862 | √ | | √ |
| 168.013(40) | 167.81(5) | 338.5 | 0.014019 | 1.502 | -42.1 | 0.0448 | | √ | √ |
| 316.485(18) | 316.440(6) | 445.7 | 0.009568 | 0.92 | 30.2 | 0.0130 | | | |
| 375.043(34) | 375.045(6) | 426.7 | 0.007907 | 0.579 | 0.3 | 0.0076 | √ | | √ |
| 380.191(105) | 380.173(2) | 393.2 | 0.007818 | 0.56 | -1.6 | 0.0060 | √ | | √ |
| 392.672(75) | 392.560(5) | 474.3 | 0.007375 | 0.511 | -4.2 | 0.0090 | √ | | √ |
| | 393.136(2) | 393.2 | 0.007355 | 0.51 | -4.7 | 0.0066 | √ | | √ |
| 407.109(49) | 406.88(17) | 509.9 | 0.007008 | 0.0206 | 0.1 | 0.0162 | | √ | √ |
| 413.664(78) | 413.707(6) | 426.7 | 0.006948 | 0.443 | -8.3 | 0.0065 | √ | | √ |
| 445.583(98) | 445.740(6) | 445.7 | 0.006305 | 0.0171 | -31.1 | 0.0046 | | √ | √ |
| 606.747(44) | 606.9(2) | 777.6 | 0.004458 | 0.12 | N/A | N/A | | | |
| 617.917(19) | 617.10(10) | 720.2 | 0.004326 | 0.151 | 0.7 | 0.0110 | | √ | √ |
| | 618.334(6) | 664.5 | 0.004308 | 0.0295 | -0.2 | 0.0042 | | √ | √ |
| 625.285(40) | 624.754(5) | 637.8 | 0.004287 | 0.0088 | -1.2 | 0.0015 | | | √ |
| | 624.78(2) | 671.0 | 0.004287 | 0.146 | 1.2 | 0.0103 | | | √ |
| 632.921(69) | 633.090(6) | 633.1 | 0.004284 | 0.13 | 0.0 | 0.0144 | | √ | √ |
| 637.723(87) | 637.717(5) | 637.8 | 0.004236 | 0.0085 | -1.2 | 0.0021 | | | √ |
| | 637.795(5) | 637.8 | 0.004234 | 0.0276 | 0.7 | 0.0066 | | | √ |
| 674.208(40) | 674.00(10) | 720.2 | 0.003827 | 0.120 | -2.0 | 0.0032 | | √ | √ |
| | 674.5(2) | 777.6 | 0.003827 | 0.12 | N/A | N/A | | | |

TABLE II: Largest-cross-section transitions, as predicted by **GNASH98**, and their status in the GEANIE data analysis. Transitions listed either have $\sigma_\gamma^{(max)} \geq 50$ mb, or $\geq 5$ mb with at least one other transition from the same parent level having $\sigma_\gamma^{(max)} \geq 50$ mb.

| $E_\gamma$ (keV) | $E_x$ (keV) | $\sigma_\gamma^{(max)}$ (b) | Comment |
|---|---|---|---|
| 46.204(6) | 46.2 | 1.0119 | $E_\gamma$ too low |
| 0.0768(5) | 0.0768 | 0.9215 | $E_\gamma$ too low |
| 56.828(3) | 103.0 | 0.5990 | $E_\gamma$ too low |
| 12.963(2) | 13.0 | 0.4571 | $E_\gamma$ too low |
| 51.624(1) | 51.7 | 0.4191 | $E_\gamma$ too low |
| 67.673(10) | 170.7 | 0.3332 | $E_\gamma$ too low |
| 98.78(2) | 150.4 | 0.3146 | contaminated by U $K_{\alpha_1}$ x ray, $^{231}$Pa $\gamma$ ray |
| 42.088(4) | 171.4 | 0.2372 | $E_\gamma$ too low |
| 46.625(20) | 197.1 | 0.1989 | $E_\gamma$ too low |
| 78.422(11) | 249.1 | 0.1968 | $E_\gamma$ too low |
| 38.661(2) | 51.7 | 0.1557 | $E_\gamma$ too low |
| 54.030(4) | 225.4 | 0.1469 | $E_\gamma$ too low |
| 89.39(6) | 338.5 | 0.1306 | contaminated by Th $K_{\alpha_2}$ x ray |
| 116.258(2) | 129.3 | 0.1167 | possibly contaminated by U $KO_{2,3}$ x ray |
| 100.0[a] | 438.6 | 0.1096 | contaminated by $^{234}$U $4_1^+ \rightarrow 2_1^+$ |
| 129.297(2) | 129.3 | 0.1082 | observed |
| 68.699(3) | 81.7 | 0.0997 | $E_\gamma$ too low |
| 30.037(3) | 81.7 | 0.0978 | $E_\gamma$ too low |
| 77.598(2) | 129.3 | 0.0944 | $E_\gamma$ too low |
| 160.19(5) | 357.3 | 0.0911 | observed |
| 111.9[a] | 550.4 | 0.0794 | contaminated by U $K_{\beta_1}$ x ray |
| 65.723(19) | 291.1 | 0.0694 | $E_\gamma$ too low |
| 167.81(5) | 338.5 | 0.0604 | observed |
| 144.201(3) | 294.6 | 0.0533 | contaminated by $^{231}$Th $\gamma$ ray |
| 120.5(2) | 670.9 | 0.0518 | contaminated by $^{230}$Th $\gamma$ ray from $^{238}$U $\alpha$-decay |
| 103.032(6) | 103.0 | 0.0448 | contaminated by $^{132}$Te $\gamma$ ray |
| 124.501(11) | 170.7 | 0.0400 | possibly observed |
| 146.095(6) | 249.1 | 0.0393 | contaminated by $^{96}$Zr/$^{101}$Zr $\gamma$ ray |
| 47.560(3) | 129.3 | 0.0335 | $E_\gamma$ too low |
| 97.576(20) | 294.6 | 0.0327 | possibly contaminated by U $K_{\alpha_1}$ x ray |
| 115.370(15) | 197.1 | 0.0271 | contaminated by U $KO_{2,3}$ x ray, $^{134}$Te $\gamma$ ray |
| 68.73(2) | 150.4 | 0.0253 | $E_\gamma$ too low |
| 189.5(1) | 438.6 | 0.0087 | possibly contaminated by $^{231}$Th $\gamma$ ray |
| 211.7(2) | 550.4 | 0.0086 | contaminated by Th $^{100}$Zr $\gamma$ ray |
| 89.648(5) | 171.4 | 0.0084 | contaminated by Th $K_{\alpha_2}$ x ray |
| 96.118(5) | 225.4 | 0.0078 | contaminated by Pa $K_{\alpha_1}$ x ray |
| 119.76(2) | 291.1 | 0.0052 | contaminated by $^{101}$Nb $\gamma$ ray |

[a] Transition is in **GNASH98** calculation but not evaluated in ENSDF.

TABLE III: Calculation of the isomer-population cross section. The deduced cross section, using Eqs. 1 and 2, is listed in the last column, labeled $\sigma_m$. Only statistical uncertainties are quoted.

| $E_n$ (MeV) | $\sum_i \sigma_{i\to m}^{(meas)}$ (b) | $\sum_i \sigma_{i\to m}^{(GNASH)}$ (b) | $\sigma_m^{(GNASH)}$ (b) | $\sigma_m$ (b) |
|---|---|---|---|---|
| 2.11(4) | 0.106(9) | 0.0880 | 0.9195 | 1.110(89) |
| 2.18(4) | 0.100(8) | 0.0892 | 0.9210 | 1.035(86) |
| 2.24(4) | 0.089(8) | 0.0906 | 0.9213 | 0.901(83) |
| 2.31(4) | 0.098(9) | 0.0913 | 0.9192 | 0.983(86) |
| 2.39(4) | 0.114(9) | 0.0918 | 0.9158 | 1.142(86) |
| 2.46(5) | 0.102(9) | 0.0924 | 0.9112 | 1.010(87) |
| 2.55(5) | 0.097(9) | 0.0931 | 0.9054 | 0.947(88) |
| 2.63(5) | 0.116(10) | 0.0937 | 0.8990 | 1.111(91) |
| 2.72(5) | 0.118(9) | 0.0944 | 0.8922 | 1.118(89) |
| 2.81(6) | 0.098(9) | 0.0951 | 0.8853 | 0.912(85) |
| 2.91(6) | 0.118(9) | 0.0958 | 0.8782 | 1.079(83) |
| 3.02(6) | 0.104(9) | 0.0966 | 0.8715 | 0.943(81) |
| 3.13(7) | 0.116(9) | 0.0976 | 0.8665 | 1.034(78) |
| 3.25(7) | 0.123(9) | 0.0989 | 0.8632 | 1.073(77) |
| 3.37(7) | 0.109(9) | 0.1005 | 0.8619 | 0.931(75) |
| 3.50(8) | 0.106(8) | 0.1027 | 0.8651 | 0.892(70) |
| 3.64(8) | 0.103(8) | 0.1054 | 0.8711 | 0.854(67) |
| 3.78(9) | 0.119(9) | 0.1077 | 0.8738 | 0.962(69) |
| 3.94(9) | 0.123(8) | 0.1104 | 0.8789 | 0.983(65) |
| 4.11(10) | 0.097(8) | 0.1127 | 0.8816 | 0.757(62) |
| 4.28(11) | 0.091(8) | 0.1150 | 0.8833 | 0.702(64) |
| 4.47(11) | 0.114(8) | 0.1173 | 0.8840 | 0.859(62) |
| 4.67(12) | 0.114(8) | 0.1195 | 0.8837 | 0.844(61) |
| 4.88(13) | 0.114(8) | 0.1215 | 0.8817 | 0.830(59) |
| 5.11(14) | 0.115(8) | 0.1230 | 0.8752 | 0.817(58) |
| 5.36(15) | 0.129(8) | 0.1220 | 0.8509 | 0.902(57) |
| 5.62(16) | 0.097(8) | 0.1218 | 0.7867 | 0.629(52) |
| 5.90(17) | 0.115(8) | 0.1090 | 0.6682 | 0.702(51) |
| 6.21(18) | 0.098(8) | 0.0926 | 0.5390 | 0.572(48) |
| 6.54(20) | 0.100(8) | 0.0775 | 0.4283 | 0.550(46) |
| 6.90(22) | 0.082(9) | 0.0646 | 0.3364 | 0.425(45) |
| 7.28(24) | 0.076(9) | 0.0555 | 0.2619 | 0.358(42) |
| 7.70(26) | 0.057(9) | 0.0463 | 0.2052 | 0.255(39) |
| 8.16(28) | 0.042(9) | 0.0380 | 0.1604 | 0.175(37) |
| 8.67(30) | 0.042(9) | 0.0308 | 0.1252 | 0.171(36) |
| 9.21(34) | 0.049(8) | 0.0250 | 0.0996 | 0.197(32) |
| 9.82(37) | 0.037(9) | 0.0205 | 0.0811 | 0.146(37) |
| 10.49(41) | 0.016(6) | 0.0171 | 0.0679 | 0.063(23) |
| 11.22(45) | 0.021(9) | 0.0147 | 0.0586 | 0.085(35) |
| 12.04(50) | 0.024(8) | 0.0129 | 0.0518 | 0.098(30) |
| 12.95(56) | 0.013(7) | 0.0115 | 0.0464 | 0.050(27) |
| 13.98(64) | 0.024(8) | 0.0103 | 0.0415 | 0.098(32) |
| 15.14(71) | 0.022(8) | 0.0092 | 0.0373 | 0.088(33) |
| 16.44(81) | 0.018(8) | 0.0083 | 0.0336 | 0.072(32) |
| 17.92(92) | 0.019(9) | 0.0074 | 0.0301 | 0.079(36) |
| 19.60(104) | 0.023(8) | 0.0064 | 0.0267 | 0.098(33) |

TABLE IV: Calculation of the ground-state-population cross section. The deduced cross section, using Eqs. 1 and 2, is listed in the last column, labeled $\sigma_g$. Only statistical uncertainties are quoted.

| $E_n$ (MeV) | $\sum_i \sigma_{i\to g}^{(meas)}$ (b) | $\sum_i \sigma_{i\to g}^{(GNASH)}$ (b) | $\sigma_g^{(GNASH)}$ (b) | $\sigma_g$ (b) |
|---|---|---|---|---|
| 2.11(4) | 0.151(6) | 0.1410 | 1.1151 | 1.190(47) |
| 2.18(4) | 0.154(6) | 0.1415 | 1.1240 | 1.223(47) |
| 2.24(4) | 0.143(6) | 0.1415 | 1.1292 | 1.142(47) |
| 2.31(4) | 0.168(6) | 0.1412 | 1.1311 | 1.340(49) |
| 2.39(4) | 0.159(6) | 0.1406 | 1.1304 | 1.269(48) |
| 2.46(5) | 0.160(6) | 0.1399 | 1.1282 | 1.285(50) |
| 2.55(5) | 0.168(6) | 0.1393 | 1.1259 | 1.354(51) |
| 2.63(5) | 0.175(7) | 0.1386 | 1.1235 | 1.414(53) |
| 2.72(5) | 0.163(6) | 0.1380 | 1.1209 | 1.322(52) |
| 2.81(6) | 0.166(6) | 0.1376 | 1.1184 | 1.348(51) |
| 2.91(6) | 0.166(6) | 0.1374 | 1.1167 | 1.349(51) |
| 3.02(6) | 0.163(6) | 0.1375 | 1.1164 | 1.327(50) |
| 3.13(7) | 0.174(6) | 0.1378 | 1.1166 | 1.414(49) |
| 3.25(7) | 0.172(6) | 0.1385 | 1.1185 | 1.396(49) |
| 3.37(7) | 0.178(6) | 0.1396 | 1.1227 | 1.437(49) |
| 3.50(8) | 0.174(6) | 0.1411 | 1.1281 | 1.398(49) |
| 3.64(8) | 0.177(6) | 0.1425 | 1.1332 | 1.415(47) |
| 3.78(9) | 0.168(6) | 0.1434 | 1.1355 | 1.336(47) |
| 3.94(9) | 0.168(6) | 0.1448 | 1.1402 | 1.350(46) |
| 4.11(10) | 0.241(12) | 0.1460 | 1.1438 | 1.493(74) |
| 4.28(11) | 0.243(12) | 0.1841 | 1.1464 | 1.509(74) |
| 4.47(11) | 0.250(12) | 0.1850 | 1.1487 | 1.542(71) |
| 4.67(12) | 0.232(11) | 0.1858 | 1.1509 | 1.427(70) |
| 4.88(13) | 0.237(12) | 0.1866 | 1.1529 | 1.448(70) |
| 5.11(14) | 0.234(11) | 0.1874 | 1.1547 | 1.430(68) |
| 5.36(15) | 0.246(11) | 0.1881 | 1.1564 | 1.513(69) |
| 5.62(16) | 0.214(11) | 0.1887 | 1.1579 | 1.309(68) |
| 5.90(17) | 0.229(11) | 0.1893 | 1.1592 | 1.449(70) |
| 6.21(18) | 0.189(11) | 0.1899 | 1.1601 | 1.257(73) |
| 6.54(20) | 0.161(11) | 0.1902 | 1.1606 | 1.124(78) |
| 6.90(22) | 0.141(11) | 0.1902 | 1.1600 | 1.032(81) |
| 7.28(24) | 0.130(11) | 0.1898 | 1.1576 | 0.975(86) |
| 7.70(26) | 0.116(11) | 0.1885 | 1.1521 | 0.893(88) |
| 8.16(28) | 0.114(12) | 0.1861 | 1.1420 | 0.908(93) |
| 8.67(30) | 0.091(11) | 0.1962 | 1.1847 | 0.751(95) |
| 9.21(34) | 0.099(12) | 0.1911 | 1.1640 | 0.851(100) |
| 9.82(37) | 0.099(12) | 0.1846 | 1.1367 | 0.890(107) |
| 10.49(41) | 0.062(11) | 0.1770 | 1.1043 | 0.593(100) |
| 11.22(45) | 0.103(12) | 0.1688 | 1.0685 | 1.029(119) |
| 12.04(50) | 0.071(13) | 0.1605 | 1.0311 | 0.747(137) |
| 12.95(56) | 0.070(12) | 0.1524 | 0.9940 | 0.782(136) |
| 13.98(64) | 0.090(13) | 0.1445 | 0.9581 | 1.055(157) |
| 15.14(71) | 0.058(13) | 0.1373 | 0.9244 | 0.721(159) |
| 16.44(81) | 0.093(14) | 0.1307 | 0.8932 | 1.202(177) |
| 17.92(92) | 0.084(13) | 0.1246 | 0.8641 | 1.134(175) |
| 19.60(104) | 0.069(12) | 0.1189 | 0.8372 | 0.968(175) |

TABLE V: Calculation of the total-population cross section. The deduced cross section, using Eqs. 1 and 2, is listed in the last column, labeled $\sigma_{g+m}$. Only statistical uncertainties are quoted.

| $E_n$ (MeV) | $\sum_i \sigma^{(meas)}_{i\to g+m}$ (b) | $\sum_i \sigma^{(GNASH)}_{i\to g+m}$ (b) | $\sigma^{(GNASH)}_{g+m}$ (b) | $\sigma_{g+m}$ (b) |
|---|---|---|---|---|
| 2.11(4) | 0.257(10) | 0.2290 | 2.0348 | 2.281(92) |
| 2.18(4) | 0.254(10) | 0.2306 | 2.0425 | 2.253(90) |
| 2.24(4) | 0.232(10) | 0.2322 | 2.0485 | 2.047(89) |
| 2.31(4) | 0.266(11) | 0.2328 | 2.0488 | 2.337(93) |
| 2.39(4) | 0.273(11) | 0.2331 | 2.0469 | 2.398(93) |
| 2.46(5) | 0.262(11) | 0.2333 | 2.0421 | 2.297(94) |
| 2.55(5) | 0.266(11) | 0.2335 | 2.0348 | 2.315(96) |
| 2.63(5) | 0.291(12) | 0.2335 | 2.0265 | 2.526(100) |
| 2.72(5) | 0.282(11) | 0.2335 | 2.0177 | 2.434(99) |
| 2.81(6) | 0.264(11) | 0.2336 | 2.0084 | 2.272(96) |
| 2.91(6) | 0.284(11) | 0.2337 | 1.9987 | 2.426(94) |
| 3.02(6) | 0.268(11) | 0.2341 | 1.9894 | 2.275(92) |
| 3.13(7) | 0.290(11) | 0.2350 | 1.9830 | 2.451(90) |
| 3.25(7) | 0.295(11) | 0.2365 | 1.9796 | 2.469(89) |
| 3.37(7) | 0.286(11) | 0.2387 | 1.9796 | 2.374(88) |
| 3.50(8) | 0.280(10) | 0.2424 | 1.9877 | 2.294(84) |
| 3.64(8) | 0.281(10) | 0.2471 | 2.0014 | 2.274(82) |
| 3.78(9) | 0.287(10) | 0.2506 | 2.0089 | 2.300(83) |
| 3.94(9) | 0.292(10) | 0.2505 | 2.0208 | 2.351(81) |
| 4.11(10) | 0.399(15) | 0.3222 | 2.0281 | 2.509(97) |
| 4.28(11) | 0.385(16) | 0.3234 | 2.0338 | 2.423(98) |
| 4.47(11) | 0.417(15) | 0.3274 | 2.0381 | 2.593(95) |
| 4.67(12) | 0.393(15) | 0.3308 | 2.0411 | 2.426(94) |
| 4.88(13) | 0.407(15) | 0.3337 | 2.0417 | 2.493(93) |
| 5.11(14) | 0.388(15) | 0.3352 | 2.0350 | 2.358(90) |
| 5.36(15) | 0.413(15) | 0.3289 | 1.9916 | 2.502(91) |
| 5.62(16) | 0.358(15) | 0.3299 | 1.9444 | 2.110(88) |
| 5.90(17) | 0.378(15) | 0.2925 | 1.7356 | 2.246(88) |
| 6.21(18) | 0.324(15) | 0.2479 | 1.4935 | 1.950(89) |
| 6.54(20) | 0.293(15) | 0.2084 | 1.2817 | 1.800(92) |
| 6.90(22) | 0.259(15) | 0.1755 | 1.1030 | 1.628(94) |
| 7.28(24) | 0.222(15) | 0.1528 | 0.9546 | 1.386(96) |
| 7.70(26) | 0.196(15) | 0.1310 | 0.8279 | 1.238(95) |
| 8.16(28) | 0.167(16) | 0.1122 | 0.7264 | 1.083(101) |
| 8.67(30) | 0.156(15) | 0.0956 | 0.6435 | 1.049(102) |
| 9.21(34) | 0.165(15) | 0.0818 | 0.5764 | 1.160(106) |
| 9.82(37) | 0.153(16) | 0.0705 | 0.5211 | 1.131(118) |
| 10.49(41) | 0.096(13) | 0.0611 | 0.4748 | 0.746(100) |
| 11.22(45) | 0.143(15) | 0.0535 | 0.4366 | 1.167(126) |
| 12.04(50) | 0.110(16) | 0.0470 | 0.4027 | 0.943(134) |
| 12.95(56) | 0.104(15) | 0.0415 | 0.3713 | 0.934(132) |
| 13.98(64) | 0.139(17) | 0.0364 | 0.3407 | 1.297(158) |
| 15.14(71) | 0.101(16) | 0.0321 | 0.3115 | 0.985(155) |
| 16.44(81) | 0.153(17) | 0.0283 | 0.2836 | 1.535(172) |
| 17.92(92) | 0.120(17) | 0.0247 | 0.2565 | 1.243(173) |
| 19.60(104) | 0.108(16) | 0.0213 | 0.2309 | 1.173(171) |

TABLE VI: Calculation of the isomer-to-ground-state population cross section ratio ($\sigma_m/\sigma_g$), using Eq. A6. Only statistical uncertainties are quoted.

| $E_n$ (MeV) | $\sum_i \sigma^{(meas)}_{i\to g}$ | $\sum_i \sigma^{(meas)}_{i\to m}$ | $\sum_i \sigma^{(meas)}_{i\to g\&m}$ | $\rho_g$ | $\rho_{g+m}$ | $\sigma_m/\sigma_g$ |
|---|---|---|---|---|---|---|
| 2.11(4) | 0.151(6) | 0.106(9) | 0.000(0) | 0.1265 | 0.1125 | 0.916(71) |
| 2.18(4) | 0.154(6) | 0.100(8) | 0.000(0) | 0.1261 | 0.1129 | 0.843(66) |
| 2.24(4) | 0.143(6) | 0.089(8) | 0.000(0) | 0.1256 | 0.1133 | 0.793(69) |
| 2.31(4) | 0.168(6) | 0.098(9) | 0.000(0) | 0.1253 | 0.1136 | 0.744(61) |
| 2.39(4) | 0.159(6) | 0.114(9) | 0.000(0) | 0.1249 | 0.1139 | 0.889(67) |
| 2.46(5) | 0.160(6) | 0.102(9) | 0.000(0) | 0.1246 | 0.1143 | 0.788(66) |
| 2.55(5) | 0.168(6) | 0.097(9) | 0.000(0) | 0.1242 | 0.1147 | 0.710(63) |
| 2.63(5) | 0.175(7) | 0.116(10) | 0.000(0) | 0.1239 | 0.1152 | 0.787(64) |
| 2.72(5) | 0.163(6) | 0.118(9) | 0.000(0) | 0.1236 | 0.1157 | 0.841(69) |
| 2.81(6) | 0.166(6) | 0.098(9) | 0.000(0) | 0.1233 | 0.1163 | 0.685(63) |
| 2.91(6) | 0.166(6) | 0.118(9) | 0.000(0) | 0.1231 | 0.1169 | 0.799(64) |
| 3.02(6) | 0.163(6) | 0.104(9) | 0.000(0) | 0.1230 | 0.1177 | 0.715(63) |
| 3.13(7) | 0.174(6) | 0.116(9) | 0.000(0) | 0.1230 | 0.1185 | 0.733(58) |
| 3.25(7) | 0.172(6) | 0.123(9) | 0.000(0) | 0.1233 | 0.1195 | 0.769(59) |
| 3.37(7) | 0.178(6) | 0.109(9) | 0.000(0) | 0.1237 | 0.1206 | 0.652(55) |
| 3.50(8) | 0.174(6) | 0.106(8) | 0.000(0) | 0.1244 | 0.1219 | 0.642(53) |
| 3.64(8) | 0.177(6) | 0.103(8) | 0.000(0) | 0.1254 | 0.1235 | 0.607(51) |
| 3.78(9) | 0.168(6) | 0.119(9) | 0.000(0) | 0.1260 | 0.1248 | 0.722(57) |
| 3.94(9) | 0.168(6) | 0.123(8) | 0.000(0) | 0.1245 | 0.1240 | 0.742(55) |
| 4.11(10) | 0.241(12) | 0.097(8) | 0.061(6) | 0.1616 | 0.1589 | 0.680(53) |
| 4.28(11) | 0.243(12) | 0.091(8) | 0.051(6) | 0.1610 | 0.1590 | 0.606(51) |
| 4.47(11) | 0.250(12) | 0.114(8) | 0.053(6) | 0.1621 | 0.1607 | 0.682(51) |
| 4.67(12) | 0.232(11) | 0.114(8) | 0.047(6) | 0.1629 | 0.1621 | 0.700(55) |
| 4.88(13) | 0.237(12) | 0.114(8) | 0.056(6) | 0.1636 | 0.1635 | 0.721(55) |
| 5.11(14) | 0.234(11) | 0.115(8) | 0.039(5) | 0.1640 | 0.1647 | 0.649(52) |
| 5.36(15) | 0.246(11) | 0.129(8) | 0.037(5) | 0.1629 | 0.1651 | 0.654(50) |
| 5.62(16) | 0.214(11) | 0.097(8) | 0.046(5) | 0.1638 | 0.1696 | 0.612(55) |
| 5.90(17) | 0.229(11) | 0.115(8) | 0.035(5) | 0.1579 | 0.1685 | 0.550(50) |
| 6.21(18) | 0.189(11) | 0.098(8) | 0.036(5) | 0.1506 | 0.1660 | 0.552(60) |
| 6.54(20) | 0.161(11) | 0.100(8) | 0.032(5) | 0.1433 | 0.1626 | 0.601(74) |
| 6.90(22) | 0.141(11) | 0.082(9) | 0.037(5) | 0.1363 | 0.1591 | 0.578(84) |
| 7.28(24) | 0.130(11) | 0.076(9) | 0.016(5) | 0.1330 | 0.1601 | 0.421(84) |
| 7.70(26) | 0.116(11) | 0.057(9) | 0.022(4) | 0.1299 | 0.1582 | 0.386(89) |
| 8.16(28) | 0.114(12) | 0.042(9) | 0.011(6) | 0.1261 | 0.1545 | 0.192(84) |
| 8.67(30) | 0.091(11) | 0.042(9) | 0.023(4) | 0.1209 | 0.1485 | 0.396(115) |
| 9.21(34) | 0.099(12) | 0.049(8) | 0.017(6) | 0.1157 | 0.1420 | 0.362(103) |
| 9.82(37) | 0.099(12) | 0.037(9) | 0.018(6) | 0.1106 | 0.1354 | 0.270(105) |
| 10.49(41) | 0.062(11) | 0.016(6) | 0.018(5) | 0.1053 | 0.1287 | 0.258(122) |
| 11.22(45) | 0.103(12) | 0.021(9) | 0.019(5) | 0.0999 | 0.1225 | 0.134(87) |
| 12.04(50) | 0.071(13) | 0.024(8) | 0.015(5) | 0.0946 | 0.1167 | 0.261(131) |
| 12.95(56) | 0.070(12) | 0.013(7) | 0.022(5) | 0.0897 | 0.1117 | 0.195(116) |
| 13.98(64) | 0.090(13) | 0.024(8) | 0.025(7) | 0.0850 | 0.1069 | 0.230(112) |
| 15.14(71) | 0.058(13) | 0.022(8) | 0.021(5) | 0.0810 | 0.1029 | 0.367(180) |
| 16.44(81) | 0.093(14) | 0.018(8) | 0.042(7) | 0.0776 | 0.0997 | 0.277(113) |
| 17.92(92) | 0.084(13) | 0.019(9) | 0.016(6) | 0.0742 | 0.0965 | 0.096(108) |
| 19.60(104) | 0.069(12) | 0.023(8) | 0.016(6) | 0.0710 | 0.0923 | 0.211(135) |

TABLE VII: Calculation of the isomer-to-ground-state population cross section ratio ($\sigma_m/\sigma_g$), using Eq. A7. Only statistical uncertainties are quoted.

| $E_n$ (MeV) | $\sum_i \sigma_{i\to g}^{(meas)}$ | $\sum_i \sigma_{i\to m}^{(meas)}$ | $\rho_g$ | $\rho_m$ | $\sigma_m/\sigma_g$ |
|---|---|---|---|---|---|
| 2.11(4) | 0.151(6) | 0.106(9) | 0.1265 | 0.0957 | 0.932(83) |
| 2.18(4) | 0.154(6) | 0.100(8) | 0.1261 | 0.0969 | 0.846(78) |
| 2.24(4) | 0.143(6) | 0.089(8) | 0.1256 | 0.0983 | 0.789(80) |
| 2.31(4) | 0.168(6) | 0.098(9) | 0.1253 | 0.0994 | 0.734(69) |
| 2.39(4) | 0.159(6) | 0.114(9) | 0.1249 | 0.1002 | 0.900(76) |
| 2.46(5) | 0.160(6) | 0.102(9) | 0.1246 | 0.1015 | 0.786(74) |
| 2.55(5) | 0.168(6) | 0.097(9) | 0.1242 | 0.1029 | 0.699(70) |
| 2.63(5) | 0.175(7) | 0.116(10) | 0.1239 | 0.1043 | 0.786(71) |
| 2.72(5) | 0.163(6) | 0.118(9) | 0.1236 | 0.1058 | 0.846(75) |
| 2.81(6) | 0.166(6) | 0.098(9) | 0.1233 | 0.1074 | 0.677(68) |
| 2.91(6) | 0.166(6) | 0.118(9) | 0.1231 | 0.1090 | 0.800(69) |
| 3.02(6) | 0.163(6) | 0.104(9) | 0.1230 | 0.1108 | 0.711(67) |
| 3.13(7) | 0.174(6) | 0.116(9) | 0.1230 | 0.1127 | 0.731(61) |
| 3.25(7) | 0.172(6) | 0.123(9) | 0.1233 | 0.1146 | 0.769(61) |
| 3.37(7) | 0.178(6) | 0.109(9) | 0.1237 | 0.1166 | 0.648(56) |
| 3.50(8) | 0.174(6) | 0.106(8) | 0.1244 | 0.1188 | 0.638(55) |
| 3.64(8) | 0.177(6) | 0.103(8) | 0.1254 | 0.1210 | 0.604(52) |
| 3.78(9) | 0.168(6) | 0.119(9) | 0.1260 | 0.1233 | 0.720(58) |
| 3.94(9) | 0.168(6) | 0.123(8) | 0.1245 | 0.1256 | 0.728(54) |
| 4.11(10) | 0.241(12) | 0.097(8) | 0.1616 | 0.1279 | 0.507(49) |
| 4.28(11) | 0.243(12) | 0.091(8) | 0.1610 | 0.1302 | 0.465(48) |
| 4.47(11) | 0.250(12) | 0.114(8) | 0.1621 | 0.1327 | 0.557(48) |
| 4.67(12) | 0.232(11) | 0.114(8) | 0.1629 | 0.1352 | 0.592(52) |
| 4.88(13) | 0.237(12) | 0.114(8) | 0.1636 | 0.1378 | 0.573(49) |
| 5.11(14) | 0.234(11) | 0.115(8) | 0.1640 | 0.1405 | 0.572(49) |
| 5.36(15) | 0.246(11) | 0.129(8) | 0.1629 | 0.1434 | 0.597(47) |
| 5.62(16) | 0.214(11) | 0.097(8) | 0.1638 | 0.1549 | 0.480(47) |
| 5.90(17) | 0.229(11) | 0.115(8) | 0.1579 | 0.1632 | 0.484(42) |
| 6.21(18) | 0.189(11) | 0.098(8) | 0.1506 | 0.1719 | 0.455(47) |
| 6.54(20) | 0.161(11) | 0.100(8) | 0.1433 | 0.1808 | 0.490(53) |
| 6.90(22) | 0.141(11) | 0.082(9) | 0.1363 | 0.1920 | 0.412(54) |
| 7.28(24) | 0.130(11) | 0.076(9) | 0.1330 | 0.2120 | 0.367(54) |
| 7.70(26) | 0.116(11) | 0.057(9) | 0.1299 | 0.2254 | 0.285(52) |
| 8.16(28) | 0.114(12) | 0.042(9) | 0.1261 | 0.2372 | 0.193(45) |
| 8.67(30) | 0.091(11) | 0.042(9) | 0.1209 | 0.2458 | 0.227(56) |
| 9.21(34) | 0.099(12) | 0.049(8) | 0.1157 | 0.2507 | 0.231(46) |
| 9.82(37) | 0.099(12) | 0.037(9) | 0.1106 | 0.2526 | 0.164(46) |
| 10.49(41) | 0.062(11) | 0.016(6) | 0.1053 | 0.2523 | 0.107(43) |
| 11.22(45) | 0.103(12) | 0.021(9) | 0.0999 | 0.2512 | 0.083(35) |
| 12.04(50) | 0.071(13) | 0.024(8) | 0.0946 | 0.2498 | 0.131(47) |
| 12.95(56) | 0.070(12) | 0.013(7) | 0.0897 | 0.2485 | 0.065(36) |
| 13.98(64) | 0.090(13) | 0.024(8) | 0.0850 | 0.2477 | 0.093(33) |
| 15.14(71) | 0.058(13) | 0.022(8) | 0.0810 | 0.2470 | 0.121(53) |
| 16.44(81) | 0.093(14) | 0.018(8) | 0.0776 | 0.2458 | 0.060(28) |
| 17.92(92) | 0.084(13) | 0.019(9) | 0.0742 | 0.2467 | 0.070(34) |
| 19.60(104) | 0.069(12) | 0.023(8) | 0.0710 | 0.2387 | 0.101(39) |

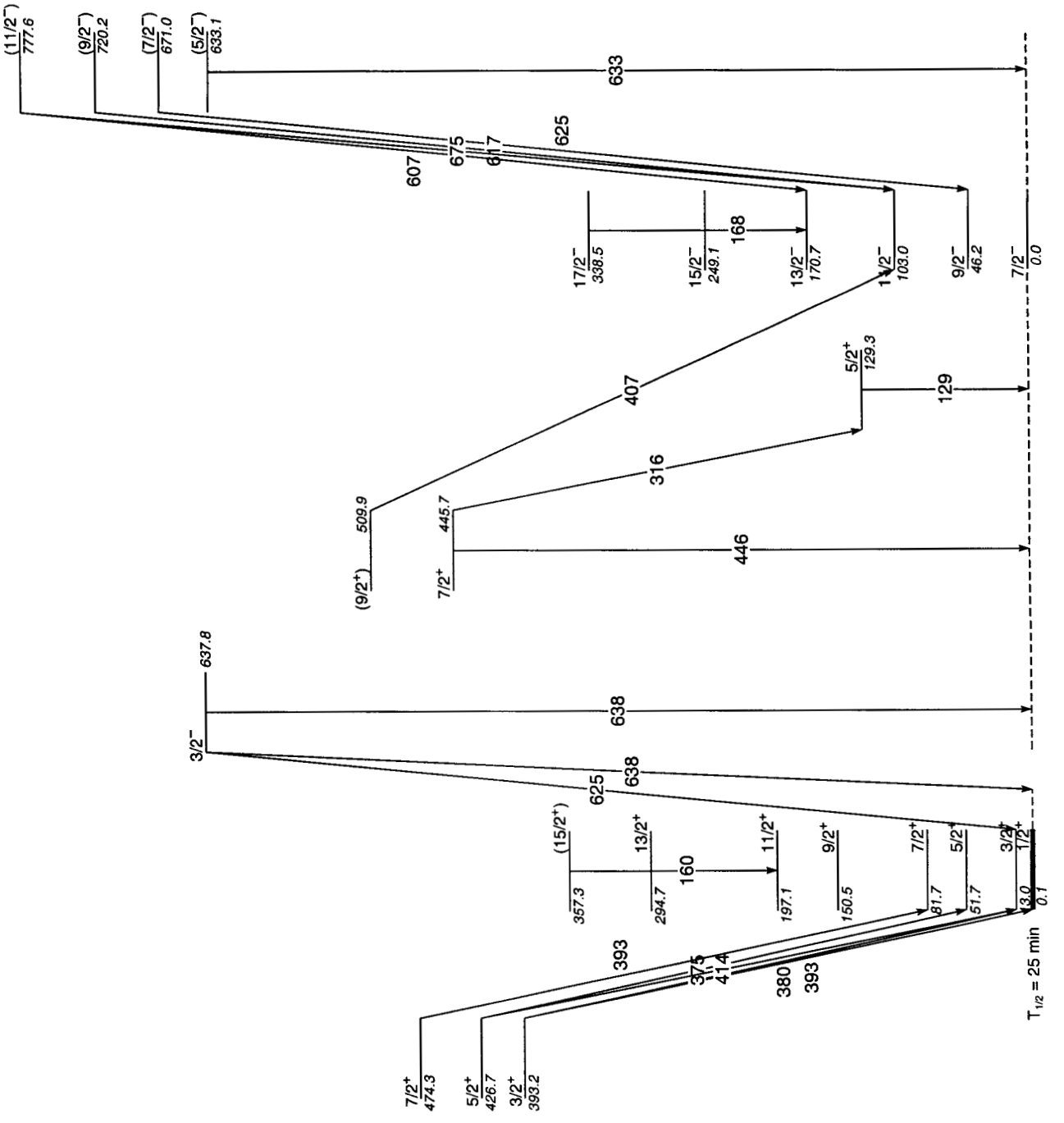


FIG. 1: Partial level scheme for $^{235}$U showing the $\gamma$ rays discussed in this report.

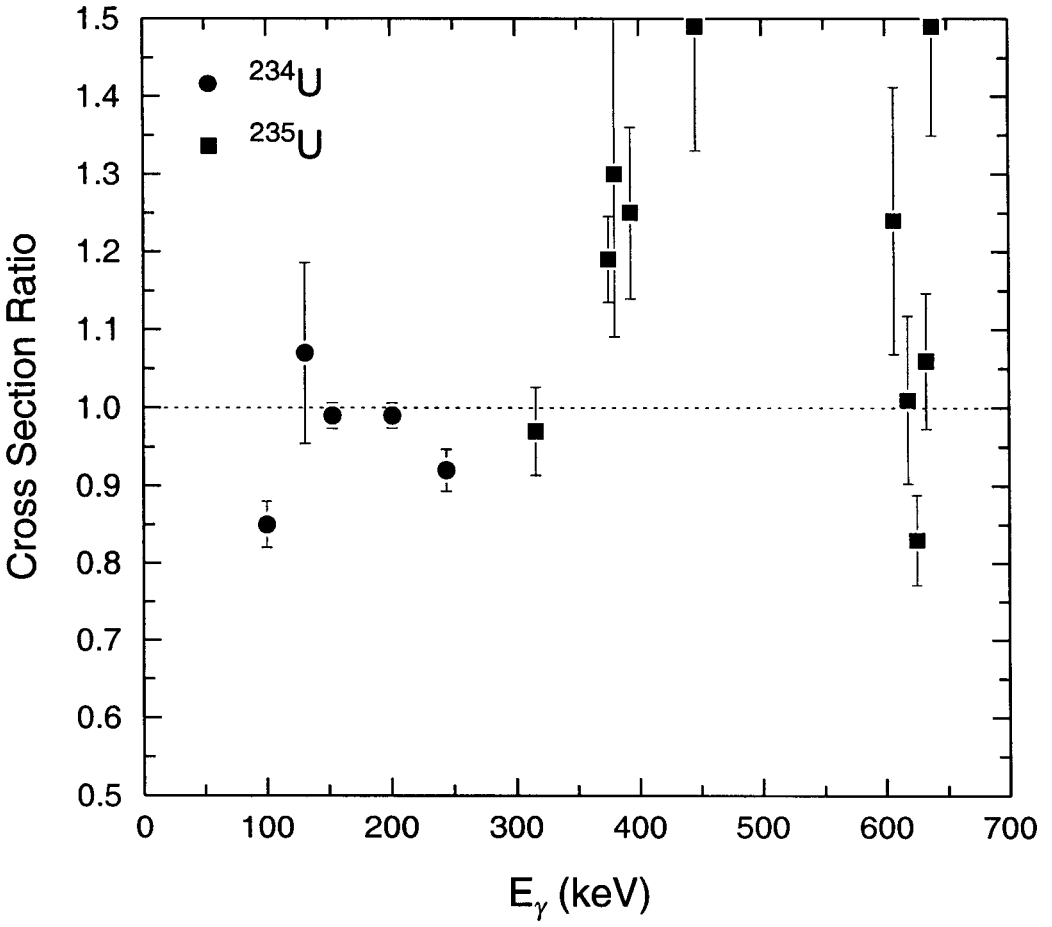


FIG. 2: Ratio of cross sections between the present data and an earlier GEANIE data set (**99Thin**), acquired with a 1.8-$\mu$s micropulse spacing. The implications of this plot for the efficiency curve used in the present analysis is discussed in section IV A

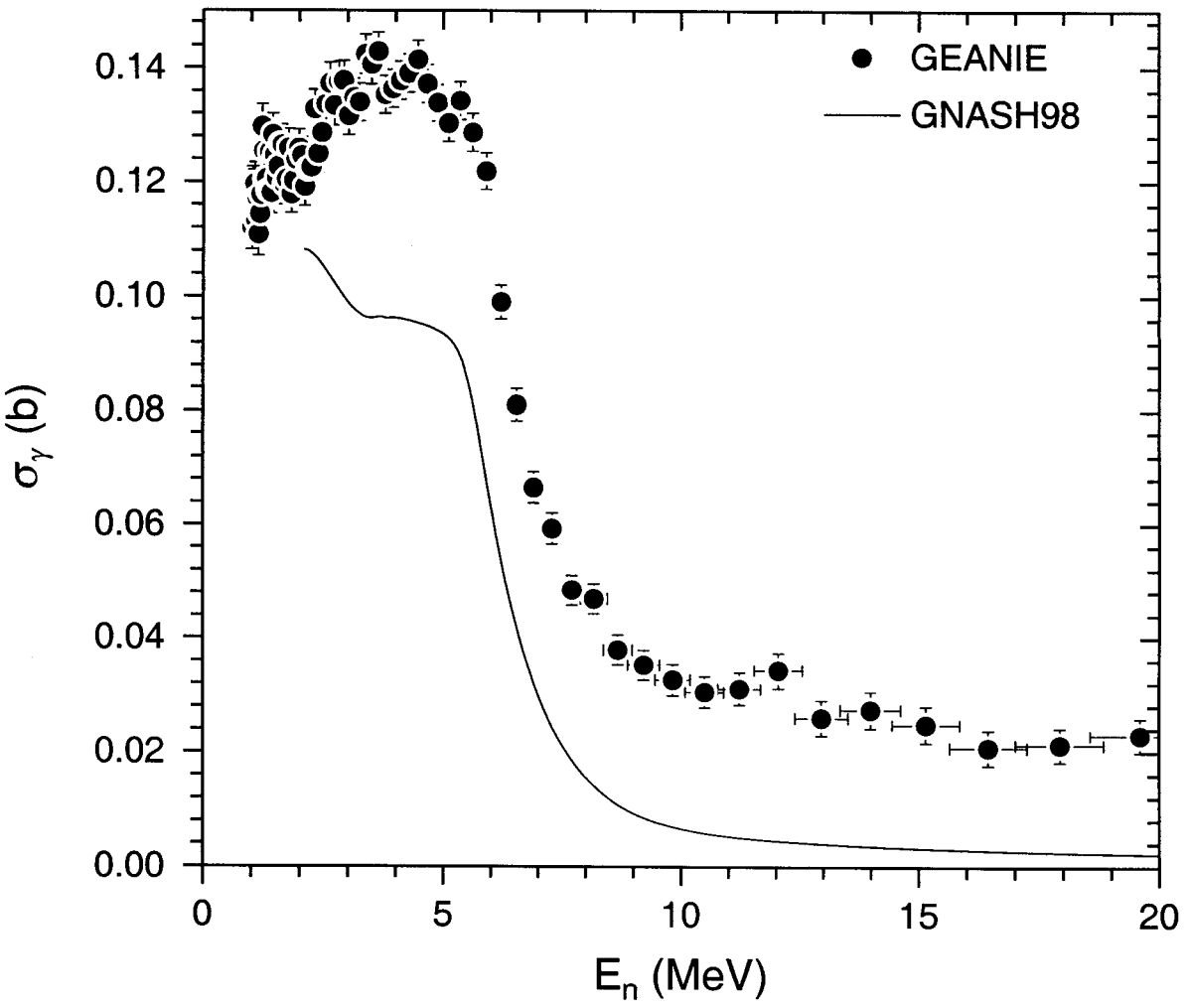


FIG. 3: Partial cross section for the $^{235}$U $E_\gamma$ = 129.3-keV transition ($E_x$=129.3 keV,$J^\pi$=$5/2^+$ → $E_x$=0.0 keV,$J^\pi$=$7/2^-$) deduced from the present data, and compared to the **GNASH98** prediction.

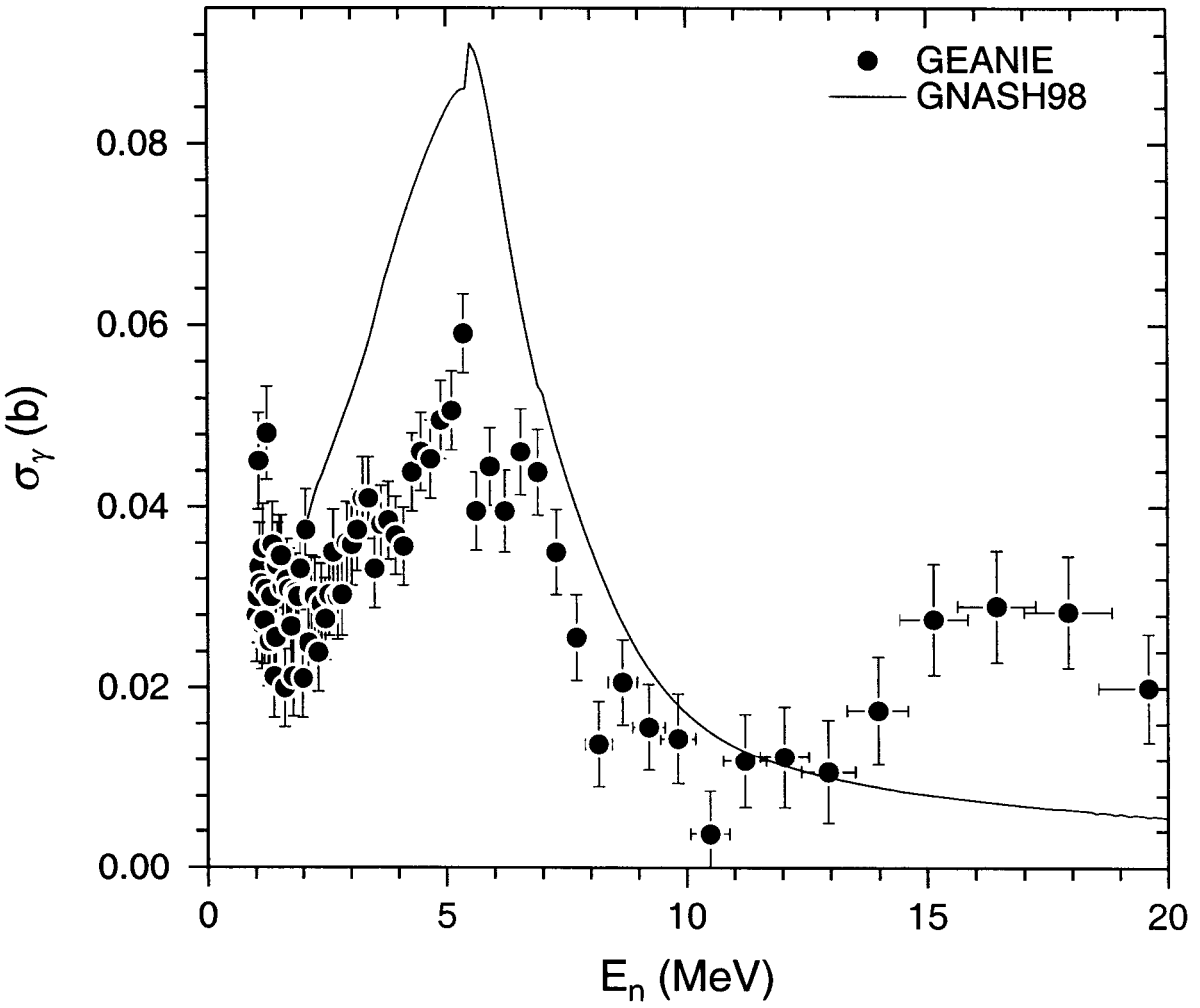


FIG. 4: Partial cross section for the $^{235}$U $E_\gamma$ = 160.2-keV transition ($E_x$=357.3 keV,$J^\pi$=$(15/2^+)$ → $E_x$=197.1 keV,$J^\pi$=$11/2^+$) deduced from the present data, and compared to the **GNASH98** prediction.

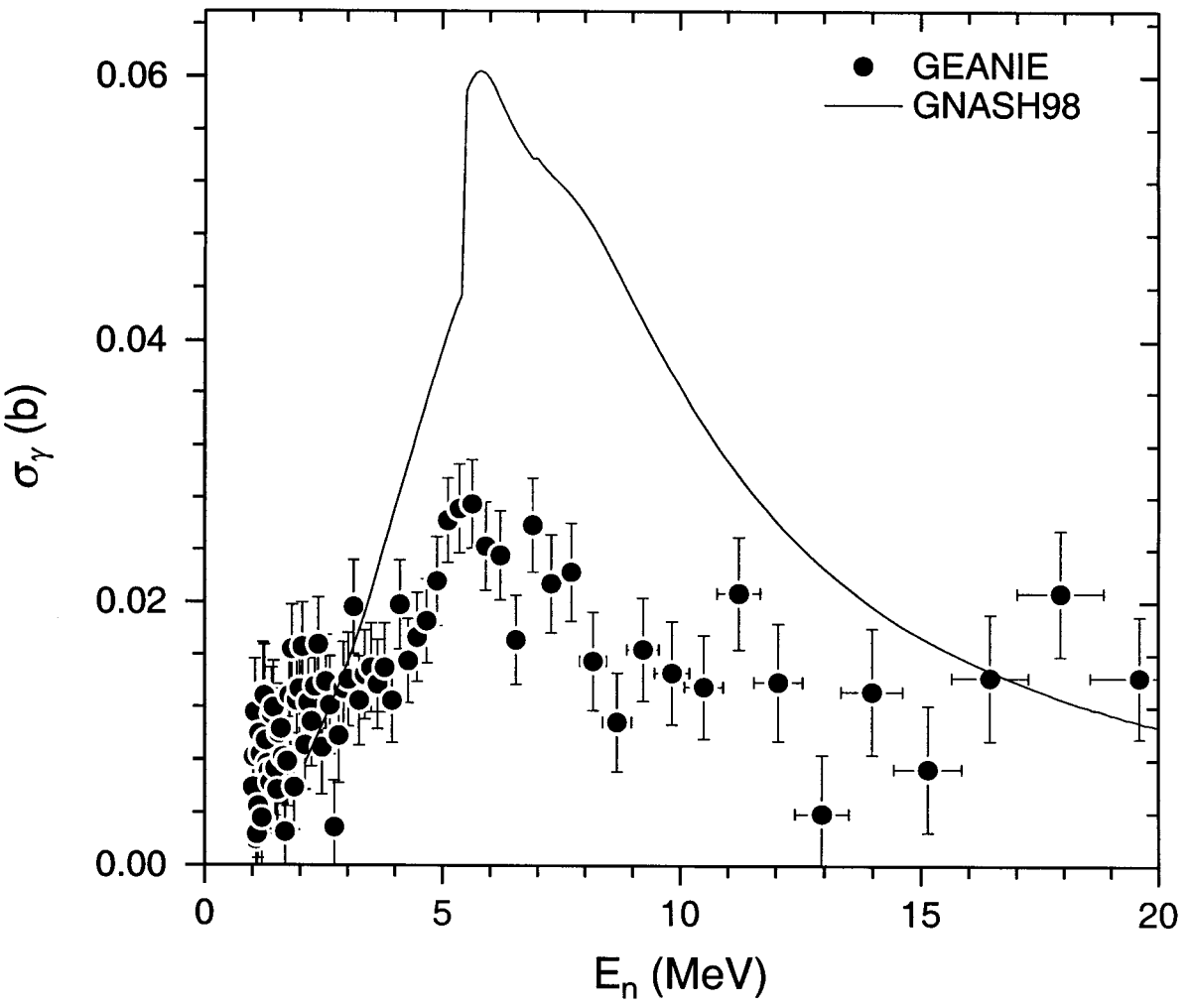


FIG. 5: Partial cross section for the $^{235}$U $E_\gamma$ = 167.8-keV transition ($E_x$=338.5 keV,$J^\pi$=17/2$^-$ → $E_x$=170.7 keV,$J^\pi$=13/2$^-$) deduced from the present data, and compared to the **GNASH98** prediction.

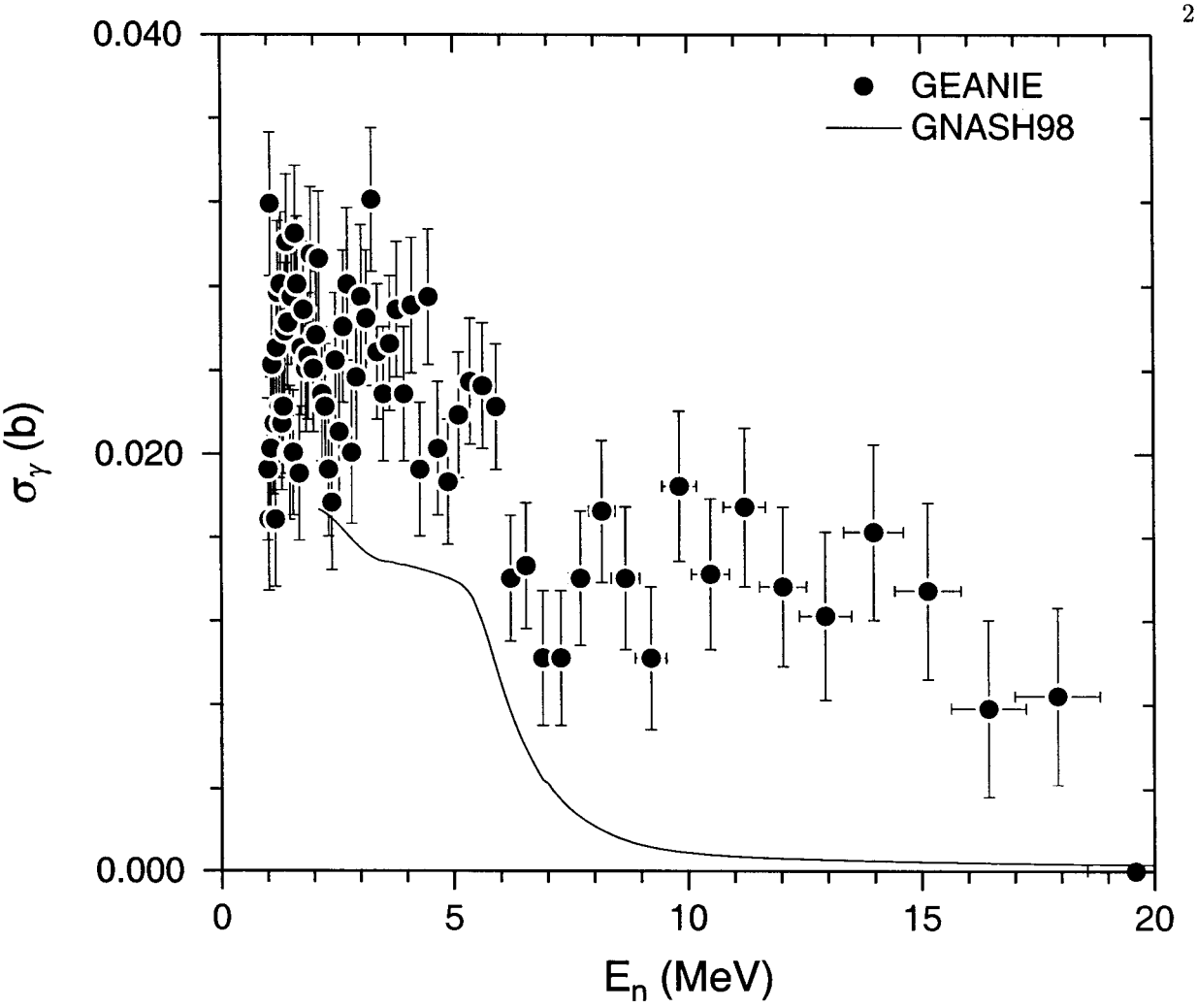


FIG. 6: Partial cross section for the $^{235}$U $E_\gamma$ = 316.4-keV transition ($E_x$=445.7 keV,$J^\pi$=$7/2^+$ → $E_x$=129.3 keV,$J^\pi$=$5/2^+$) deduced from the present data, and compared to the **GNASH98** prediction.

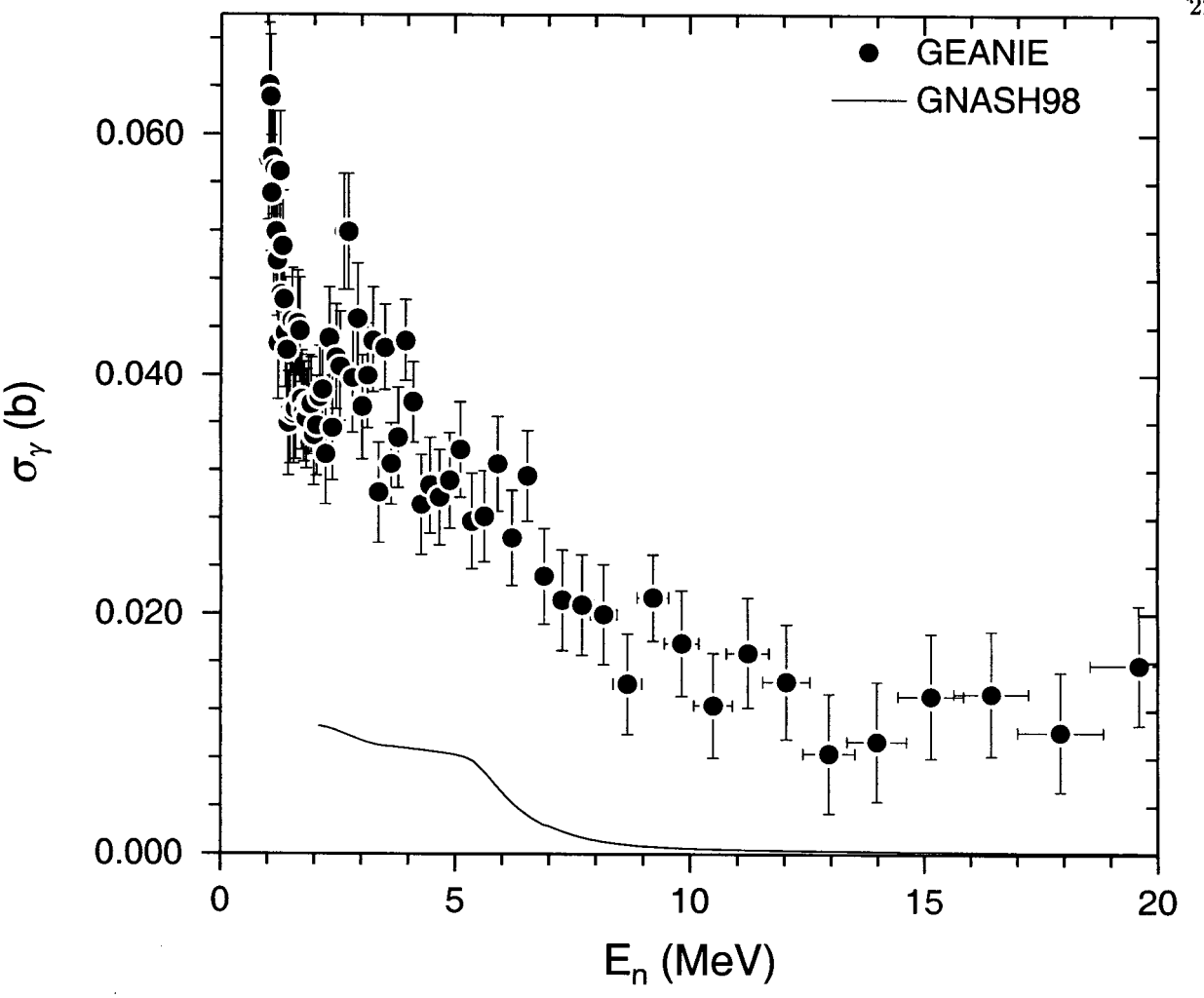


FIG. 7: Partial cross section for the $^{235}$U $E_\gamma$ = 375.0-keV transition ($E_x$=426.7 keV,$J^\pi$=$5/2^+$ → $E_x$=51.7 keV,$J^\pi$=$5/2^+$) deduced from the present data, and compared to the **GNASH98** prediction.

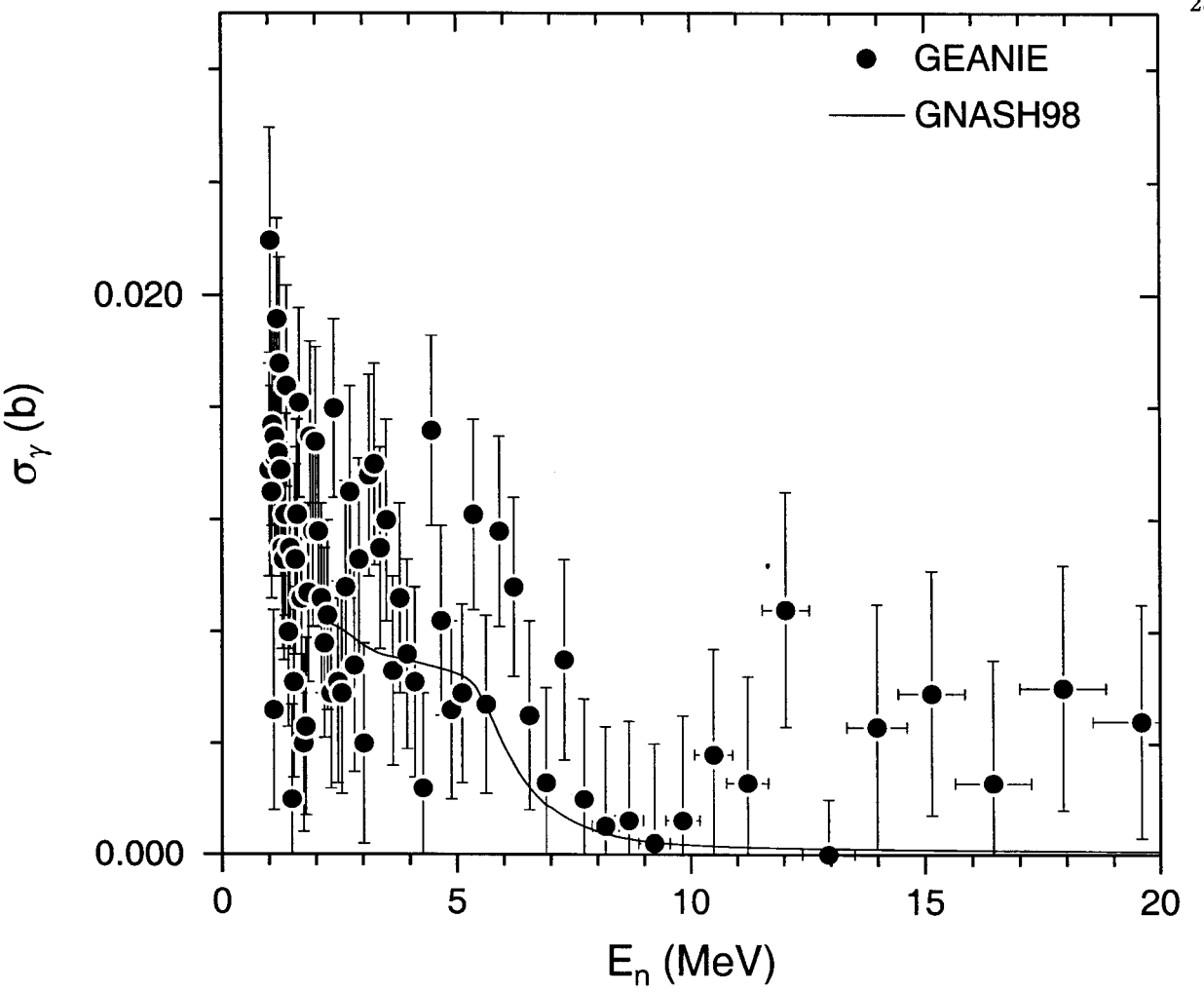


FIG. 8: Partial cross section for the $^{235}$U $E_\gamma$ = 380.2-keV transition ($E_x$=393.2 keV,$J^\pi$=$3/2^+$ → $E_x$=13.0 keV,$J^\pi$=$3/2^+$) deduced from the present data, and compared to the **GNASH98** prediction.

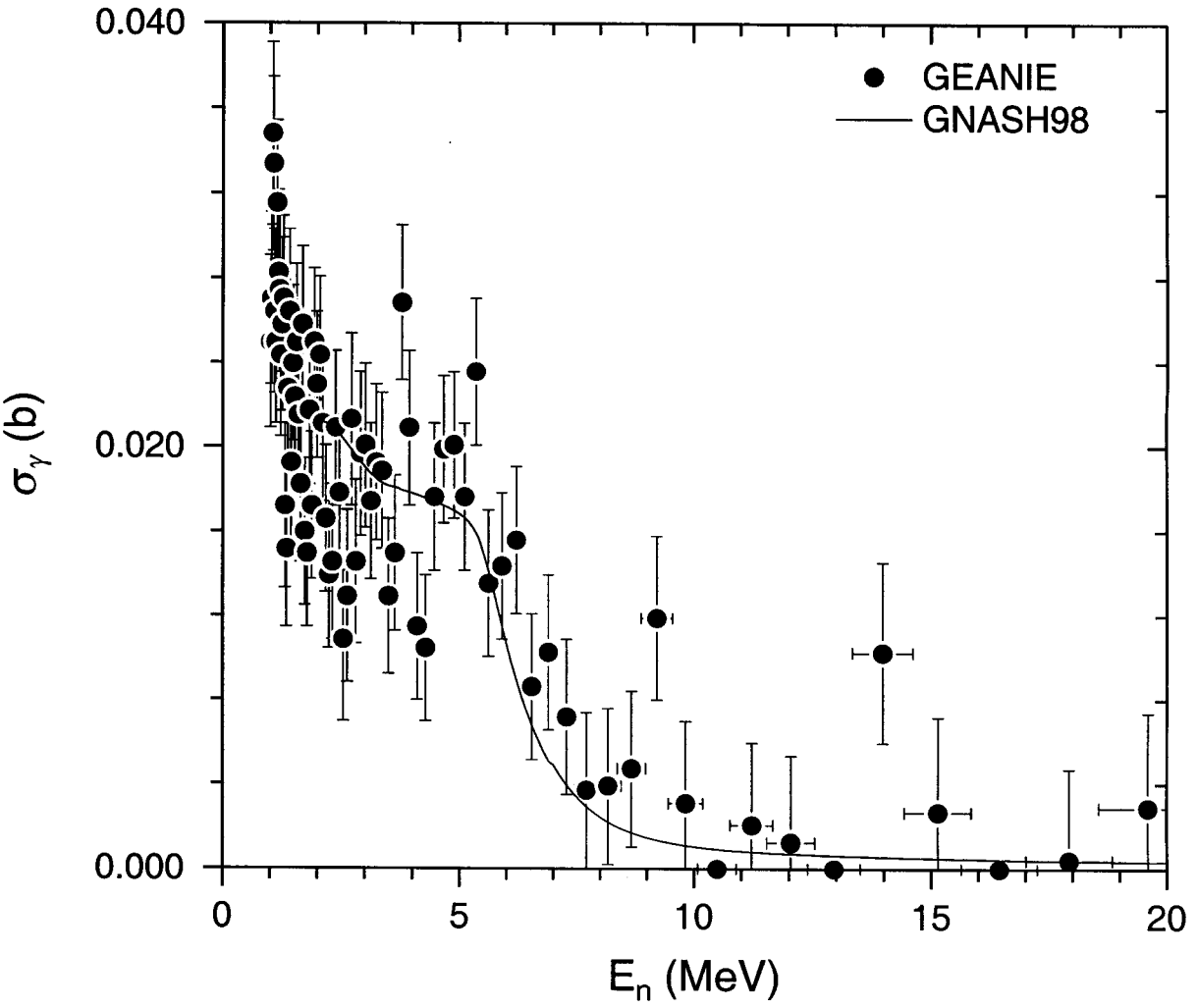


FIG. 9: Partial cross section for the $^{235}$U $E_\gamma$ = 392.6/393.1-keV transitions ($E_x$=474.3 keV,$J^\pi$=$7/2^+$ → $E_x$=81.7 keV,$J^\pi$=$7/2^+$ and $E_x$=393.2 keV,$J^\pi$=$3/2^+$ → $E_x$=77 eV,$J^\pi$=$1/2^+$) deduced from the present data, and compared to the **GNASH98** prediction.

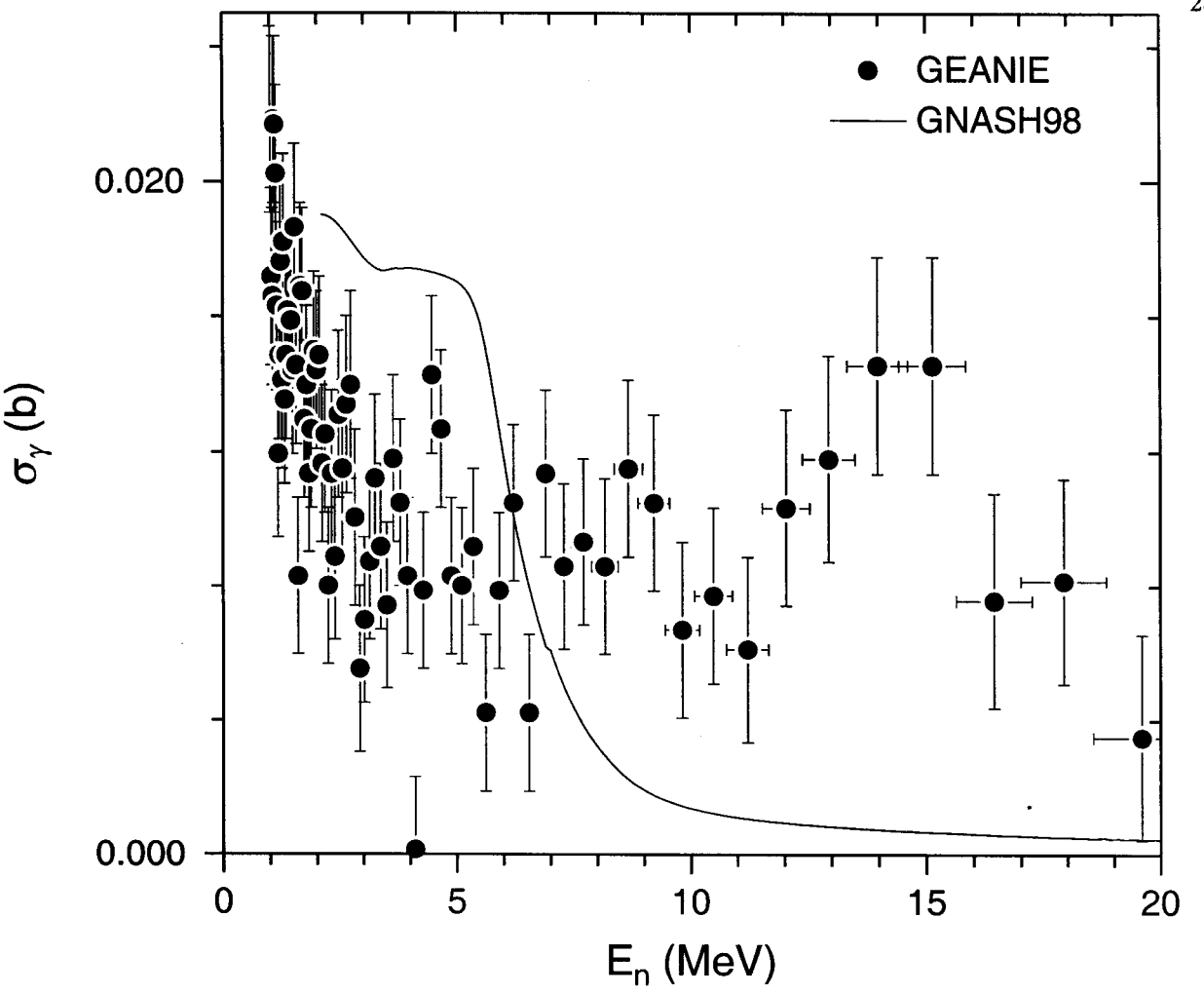


FIG. 10: Partial cross section for the $^{235}$U $E_\gamma$ = 406.9-keV transition ($E_x$=509.9 keV,$J^\pi$=$(9/2^+)$ $\rightarrow$ $E_x$=103.0 keV,$J^\pi$=$11/2^-$) deduced from the present data, and compared to the **GNASH98** prediction.

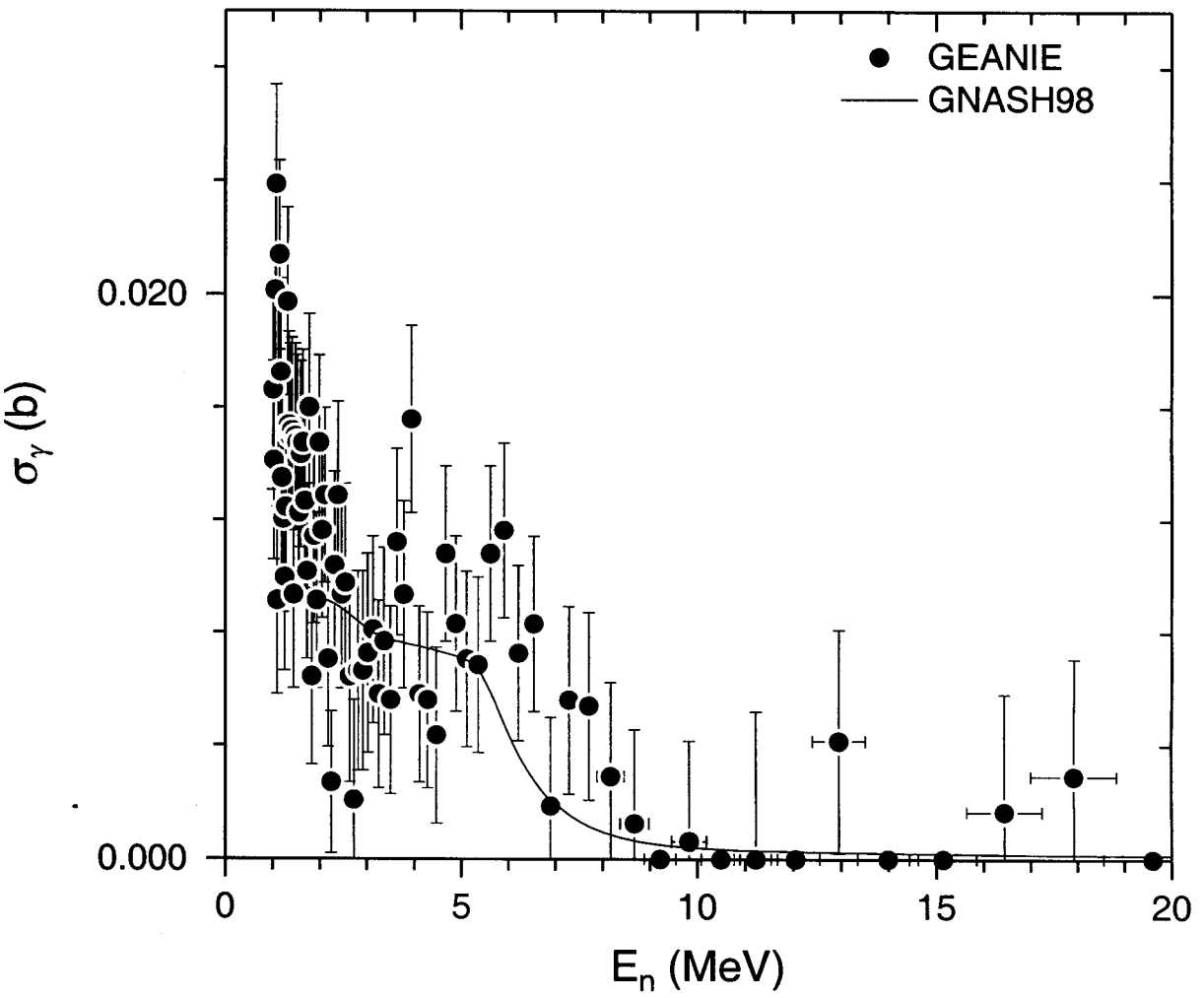


FIG. 11: Partial cross section for the $^{235}$U $E_\gamma$ = 413.7-keV transition ($E_x$=426.7 keV,$J^\pi$=$5/2^+$ → $E_x$=13.0 keV,$J^\pi$=$3/2^+$) deduced from the present data, and compared to the **GNASH98** prediction.

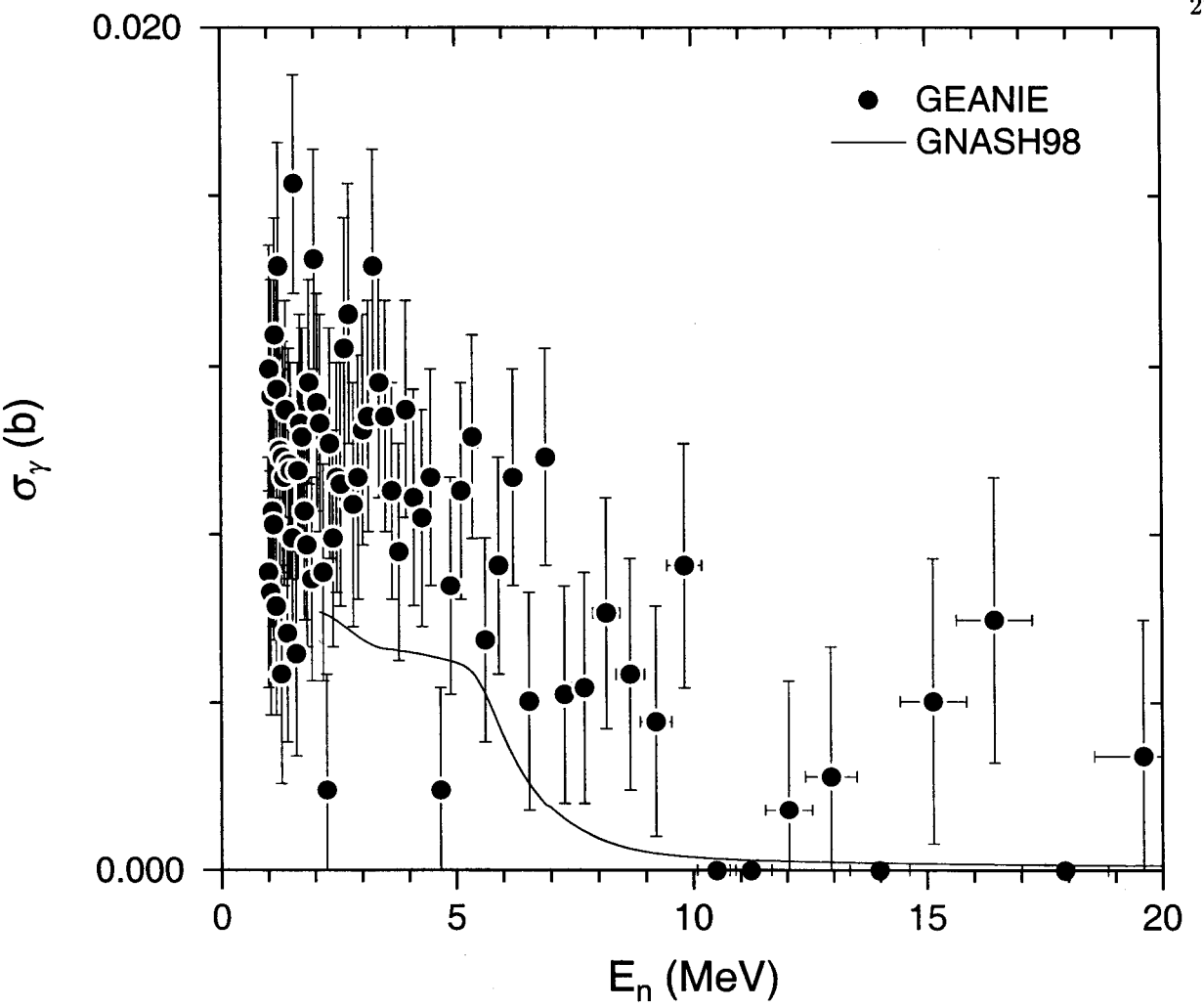


FIG. 12: Partial cross section for the $^{235}$U $E_\gamma$ = 445.7-keV transition ($E_x$=445.7 keV,$J^\pi$=$7/2^+$ → $E_x$=0.0 keV,$J^\pi$=$7/2^-$) deduced from the present data, and compared to the **GNASH98** prediction.

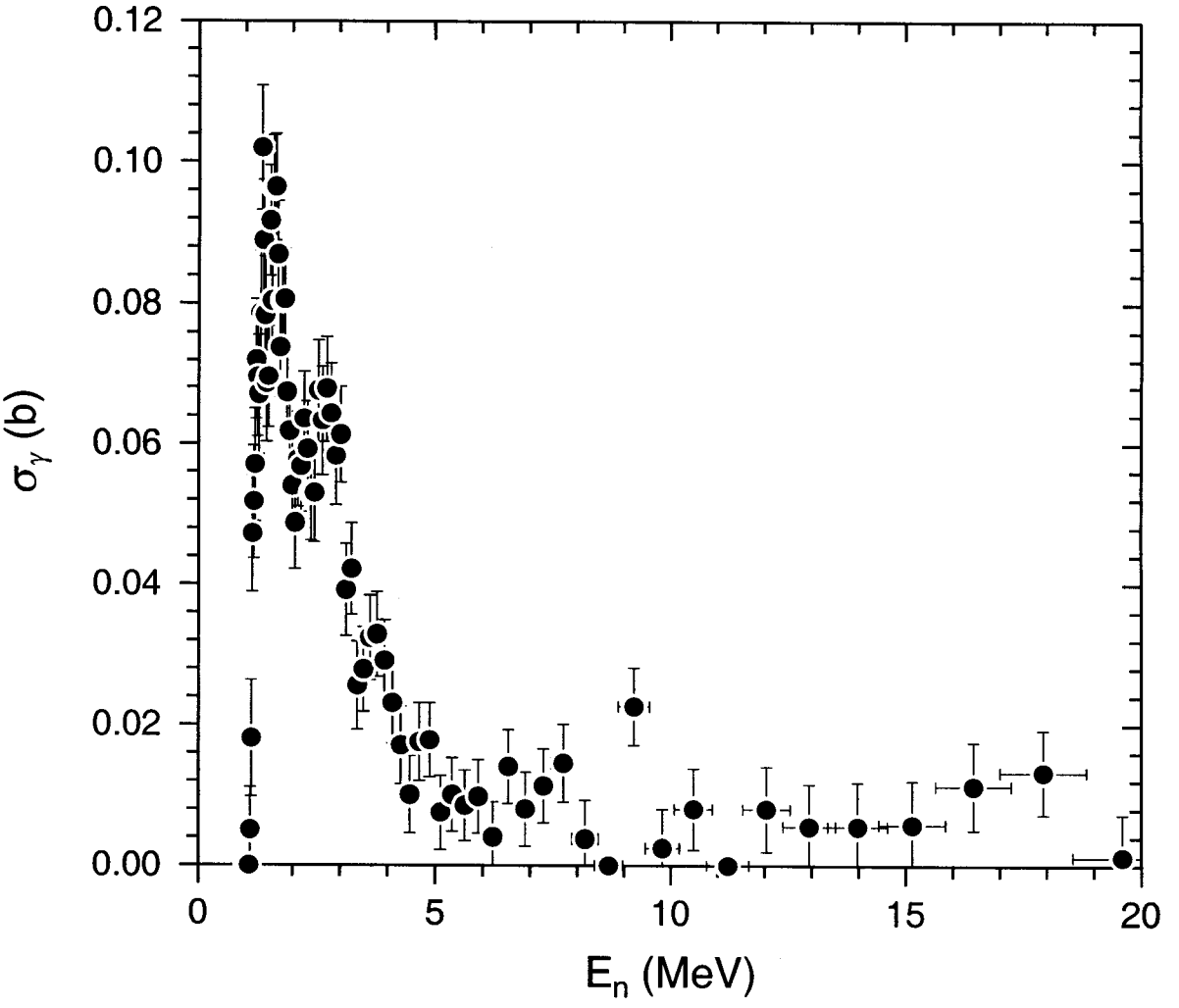


FIG. 13: Partial cross section for the $^{235}$U $E_\gamma$ = 606.9-keV transition ($E_x$=777.6 keV,$J^\pi$=$(11/2^-)$ → $E_x$=170.7 keV,$J^\pi$=$13/2^-$) deduced from the present data. No **GNASH98** prediction is available for this line. The peak in cross section in the $E_n$ = 2-4-MeV range is due to an artifact of the fit (see text).

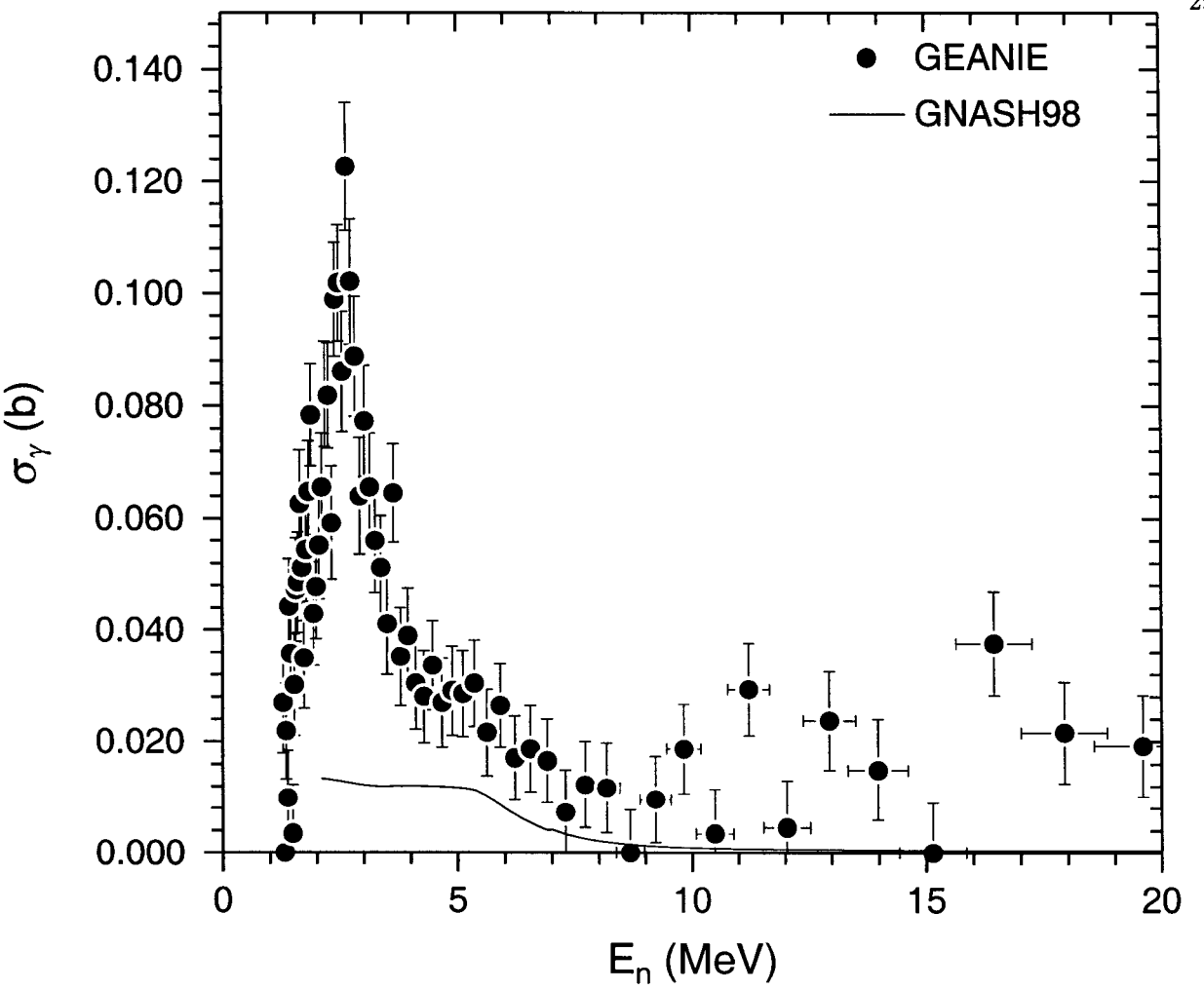


FIG. 14: Partial cross section for the $^{235}$U $E_\gamma$ = 617.1-keV transition ($E_x$=720.2 keV,$J^\pi$=$(9/2^-)$ → $E_x$=103.0 keV,$J^\pi$=$11/2^-$) deduced from the present data, and compared to the **GNASH98** prediction. The peak in cross section in the $E_n$ = 2-4-MeV range is due to an artifact of the fit (see text).

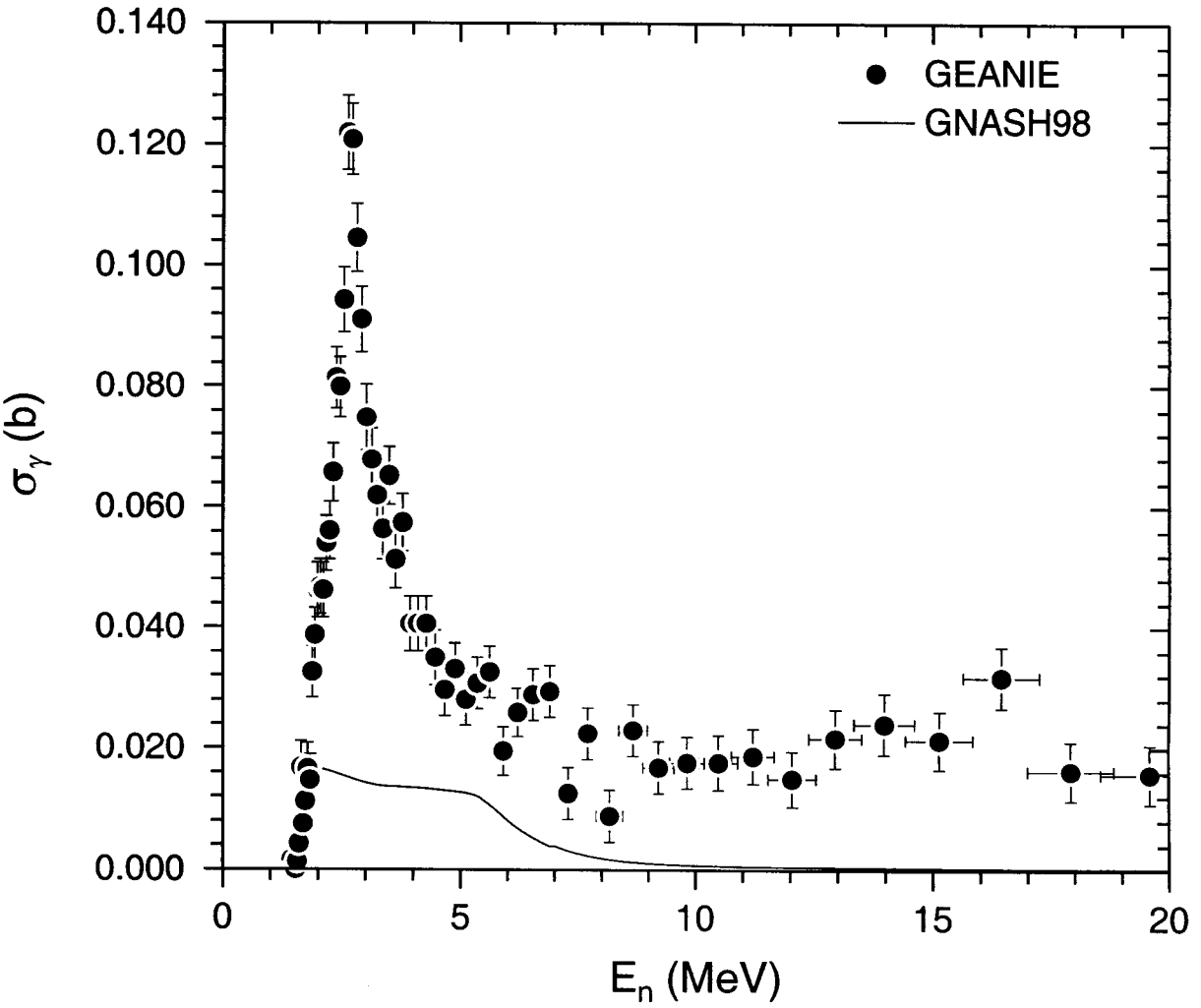


FIG. 15: Partial cross section for the $^{235}$U $E_\gamma$ = 624.8/624.8-keV transition ($E_x$=671.0 keV,$J^\pi$=(7/2$^-$) $\rightarrow$ $E_x$=46.2 keV,$J^\pi$=9/2$^-$ and $E_x$=637.8 keV,$J^\pi$=3/2$^-$ $\rightarrow$ $E_x$=13.0 keV,$J^\pi$=3/2$^+$) deduced from the present data, and compared to the **GNASH98** prediction. The peak in cross section in the $E_n$ = 2-4-MeV range is due to an artifact of the fit (see text).

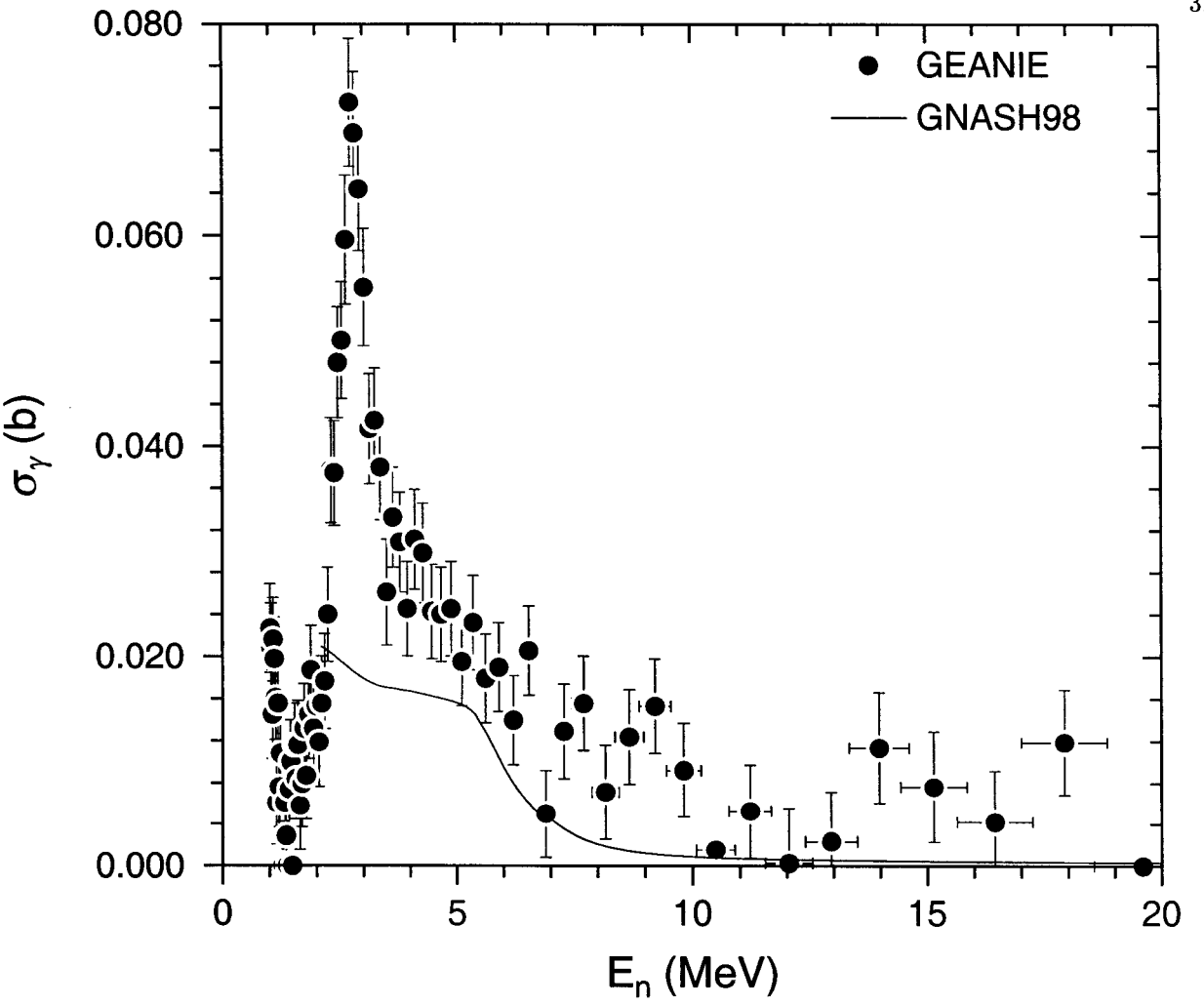


FIG. 16: Partial cross section for the $^{235}$U $E_\gamma$ = 633.1-keV transition ($E_x$=633.1 keV,$J^\pi$=(5/2$^-$) → $E_x$=0.0 keV,$J^\pi$=7/2$^-$) deduced from the present data, and compared to the **GNASH98** prediction. The peak in cross section in the $E_n$ = 2-4-MeV range is due to an artifact of the fit (see text).

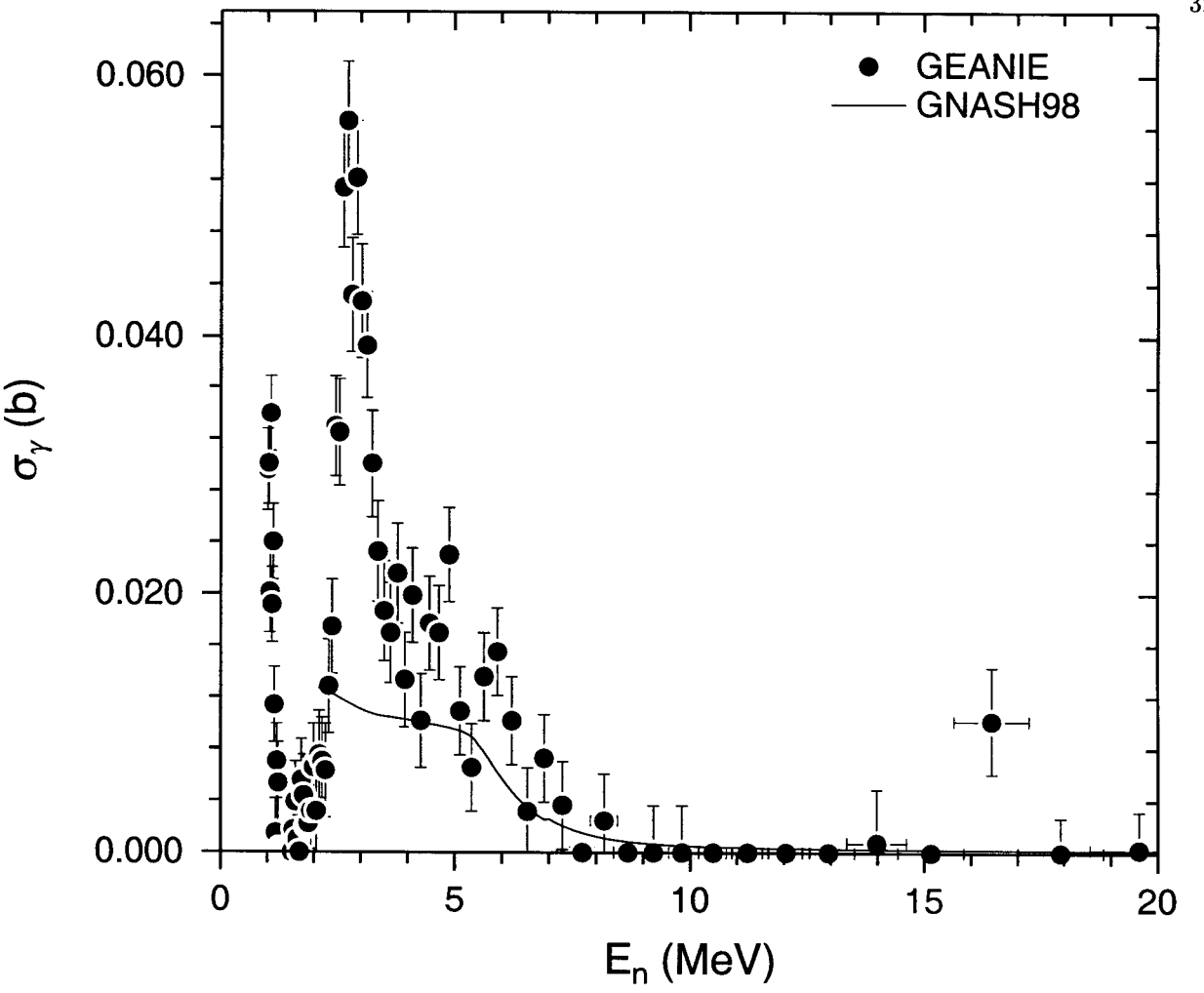


FIG. 17: Partial cross section for the $^{235}$U $E_\gamma$ = 637.7/637.8-keV transitions ($E_x$=637.8 keV,$J^\pi$=3/2$^-$ → $E_x$=77 eV,$J^\pi$=1/2$^+$ and $E_x$=637.8 keV,$J^\pi$=3/2$^-$ → $E_x$=0.0 keV,$J^\pi$=7/2$^-$) deduced from the present data, and compared to the **GNASH98** prediction. The peak in cross section in the $E_n$ = 2-4-MeV range is due to an artifact of the fit (see text).

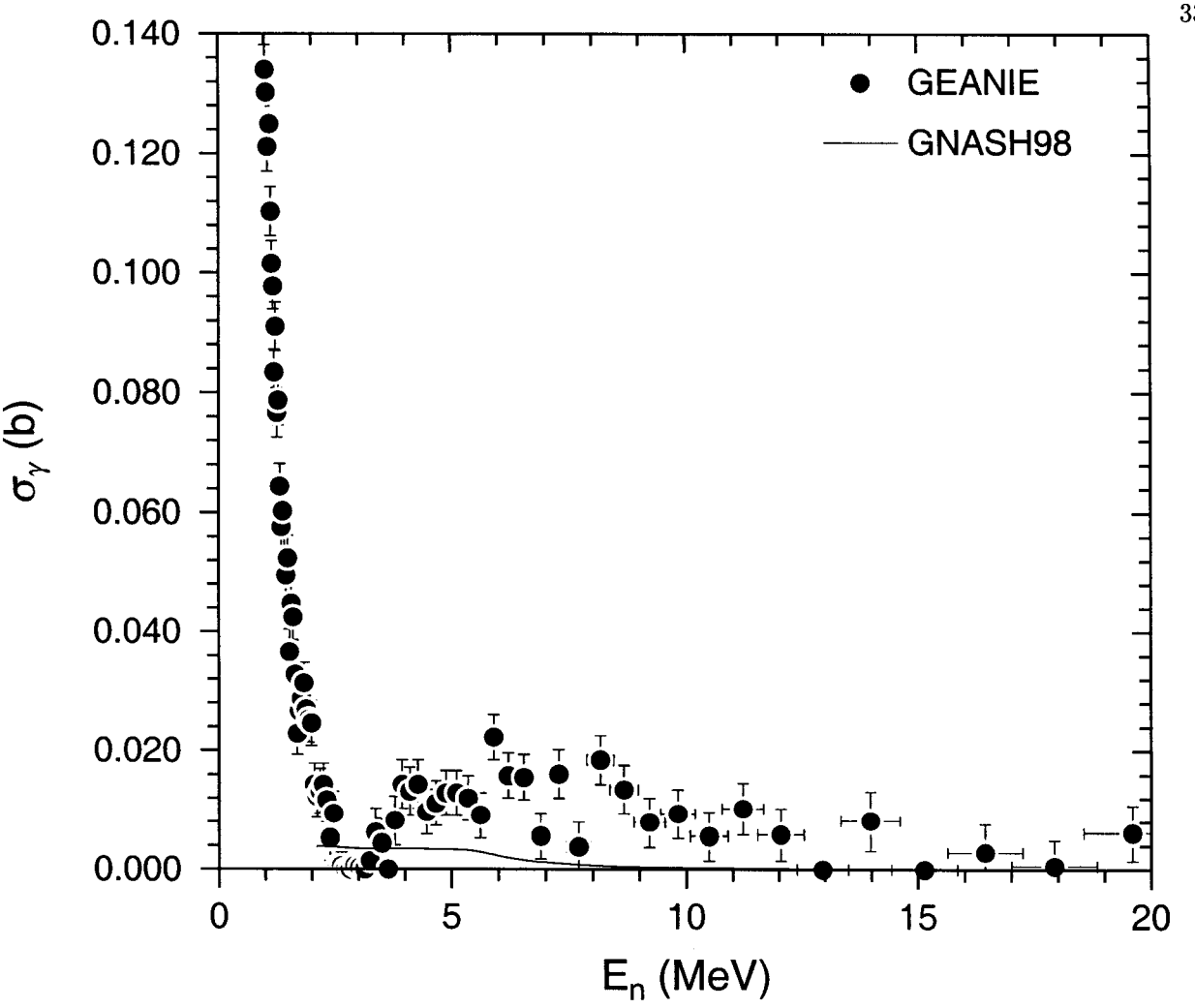


FIG. 18: Partial cross section for the $^{235}$U $E_\gamma$ = 674.0-keV transition ($E_x$=777.6 keV,$J^\pi$=$(11/2^-)$ → $E_x$=103.0 keV,$J^\pi$=$11/2^-$) deduced from the present data, and compared to the **GNASH98** prediction.

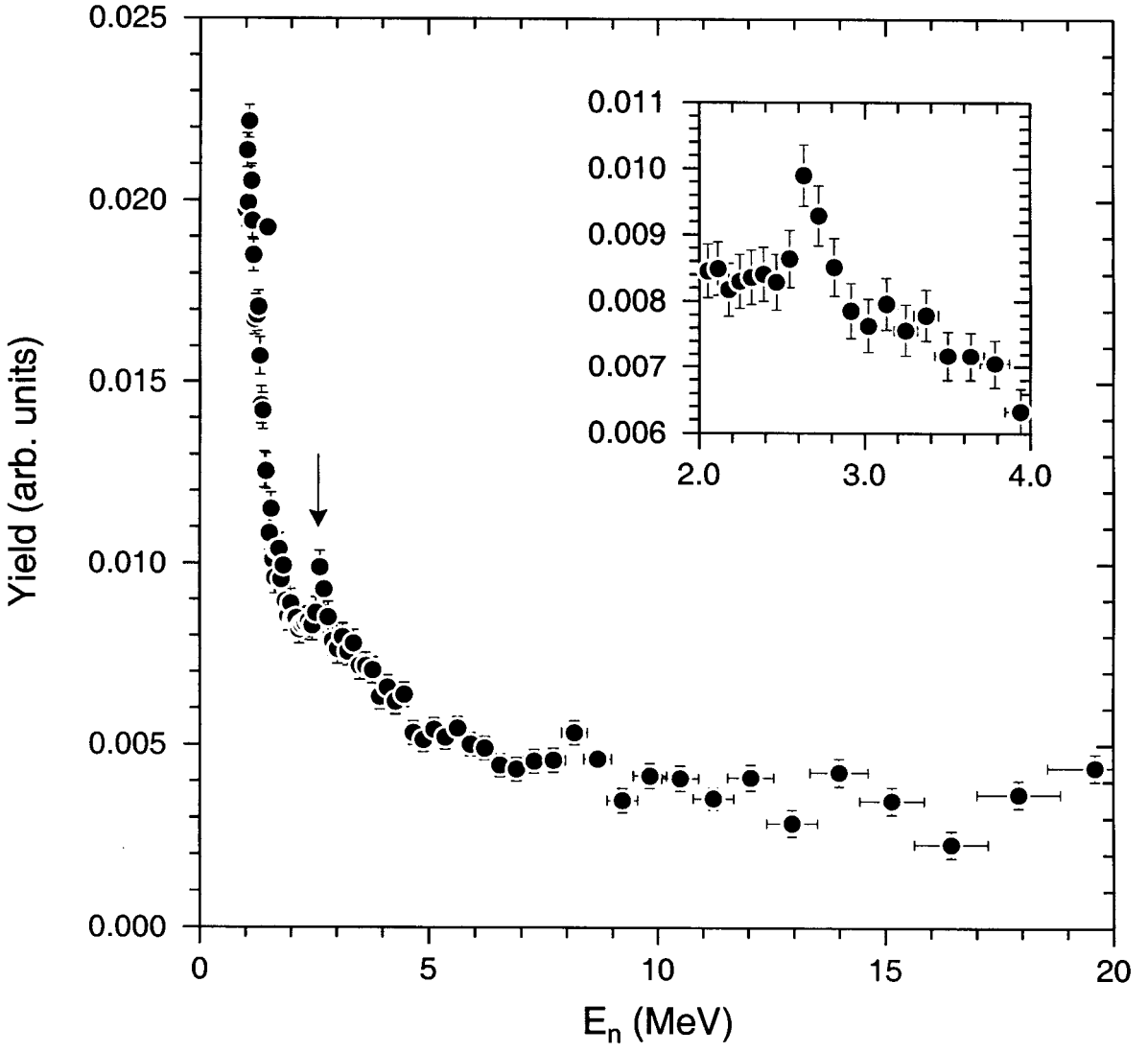


FIG. 19: Excitation function of the neutron bump arising from the $E_\gamma = 595.8$-keV transition in $^{74}$Ge. The arrow indicates a feature which is due to inadequate modeling of the neutron bump, and the inset shows an expanded view of this feature. This effect can be seen in the excitation functions for $\gamma$ rays with $590 \leq E_\gamma(\text{keV}) \leq 640$ near $E_n \approx 2.7$ MeV.

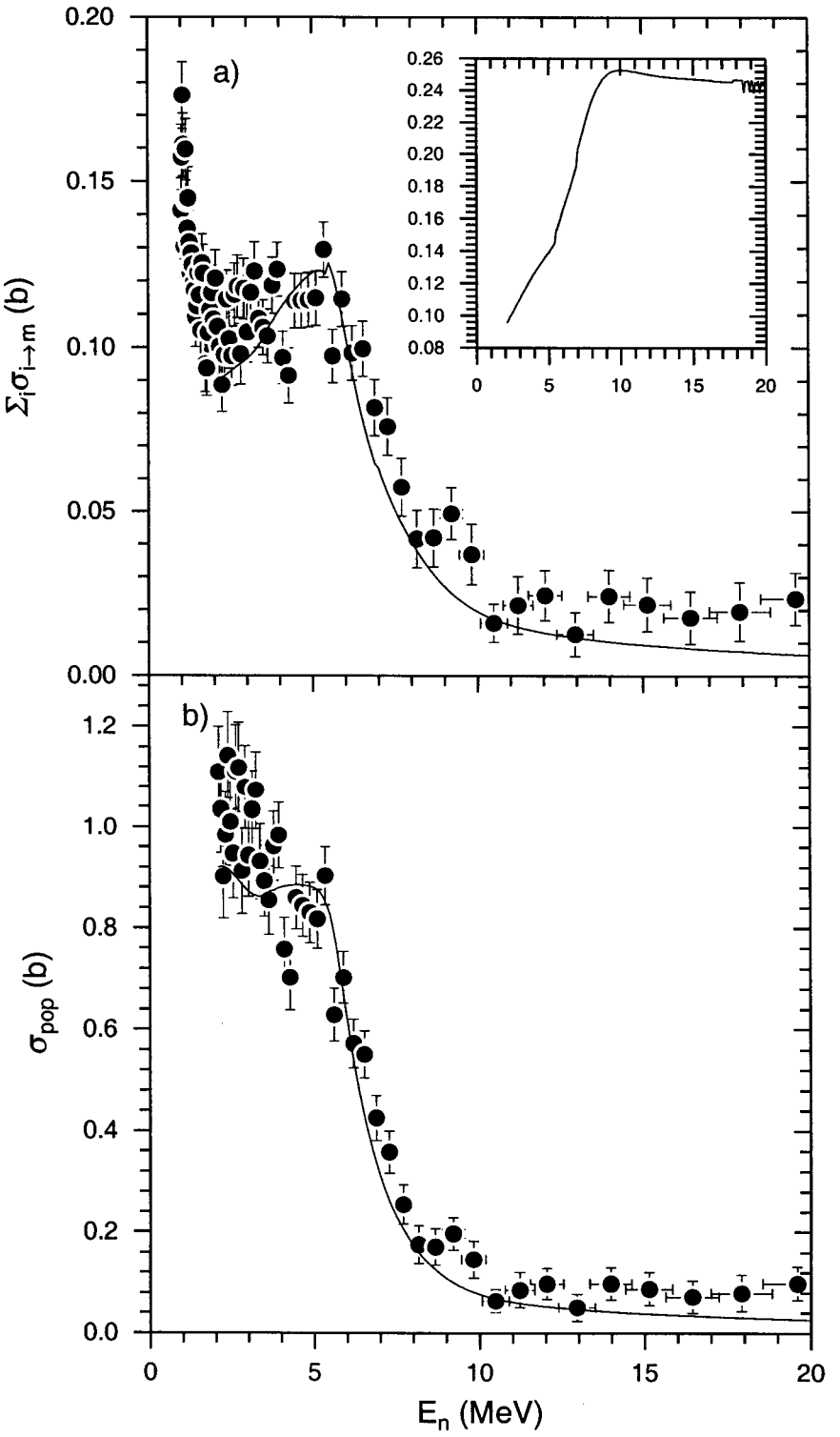


FIG. 20: Isomer-population cross section (panel b), deduced from the sum of parallel-path ($\sum_i \sigma_{i\to m}^{(meas)}$ in table I) transition cross sections (panel a) using Eqs. 1 and 2. The solid curve shows the **GNASH98** prediction in each case. The inset in panel a) shows the partial-to-total ratio, calculated in **GNASH98**, and used to deduce the population cross section.

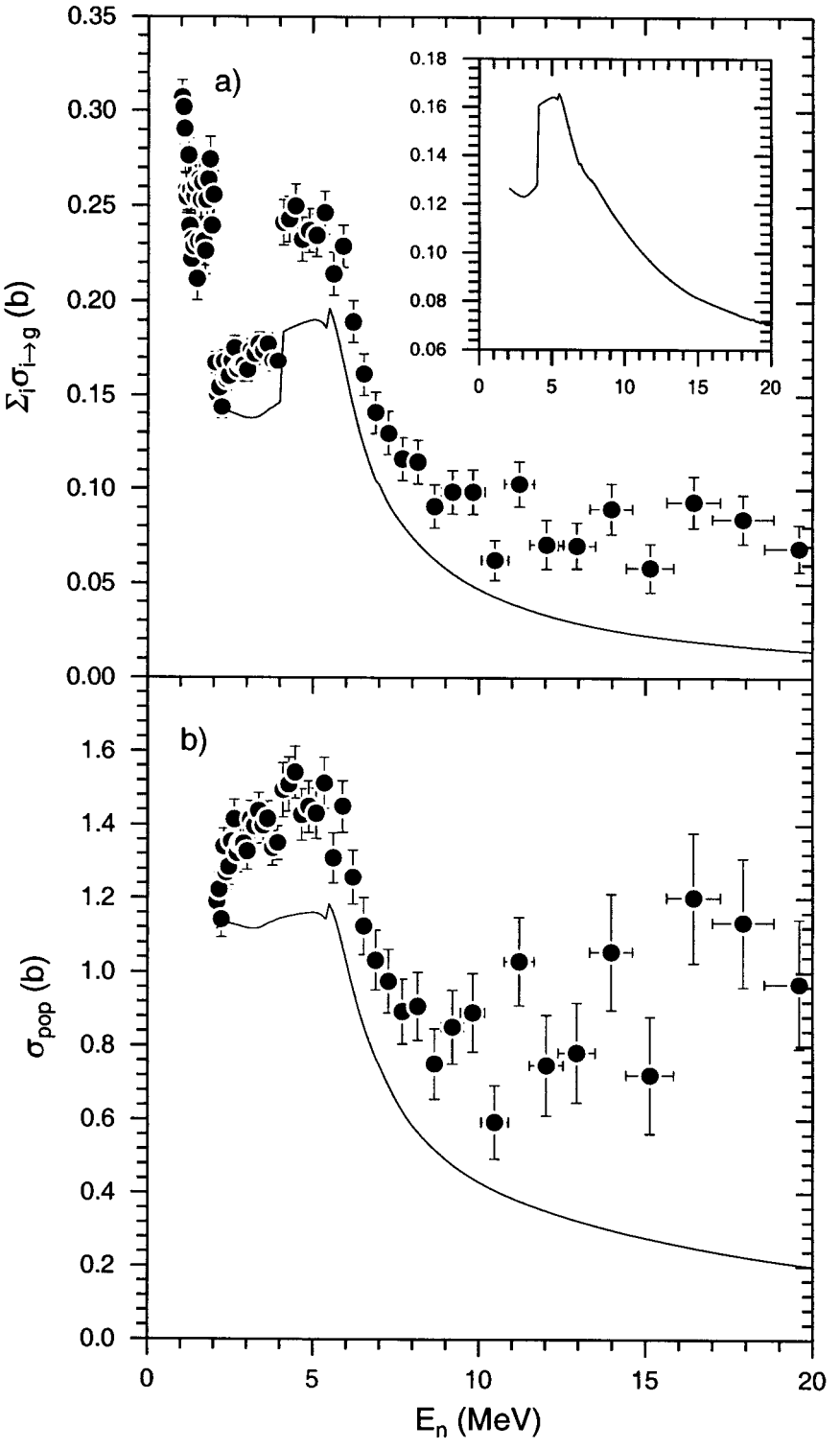


FIG. 21: Ground-State-population cross section (panel b), deduced from the sum of parallel-path ($\sum_i \sigma_{i\to g}^{(meas)}$ in table I) transition cross sections (panel a) using Eqs. 1 and 2. The solid curve shows the **GNASH98** prediction in each case. The inset in panel a) shows the partial-to-total ratio, calculated in **GNASH98**, and used to deduce the population cross section. The apparent discontinuities at $E_n$ = 2 and 4 MeV in the data in panel a) are due to the exclusion of $\gamma$ rays in the $E_\gamma$ = 590–640-keV range for $E_n$ = 2-4 MeV (see text).

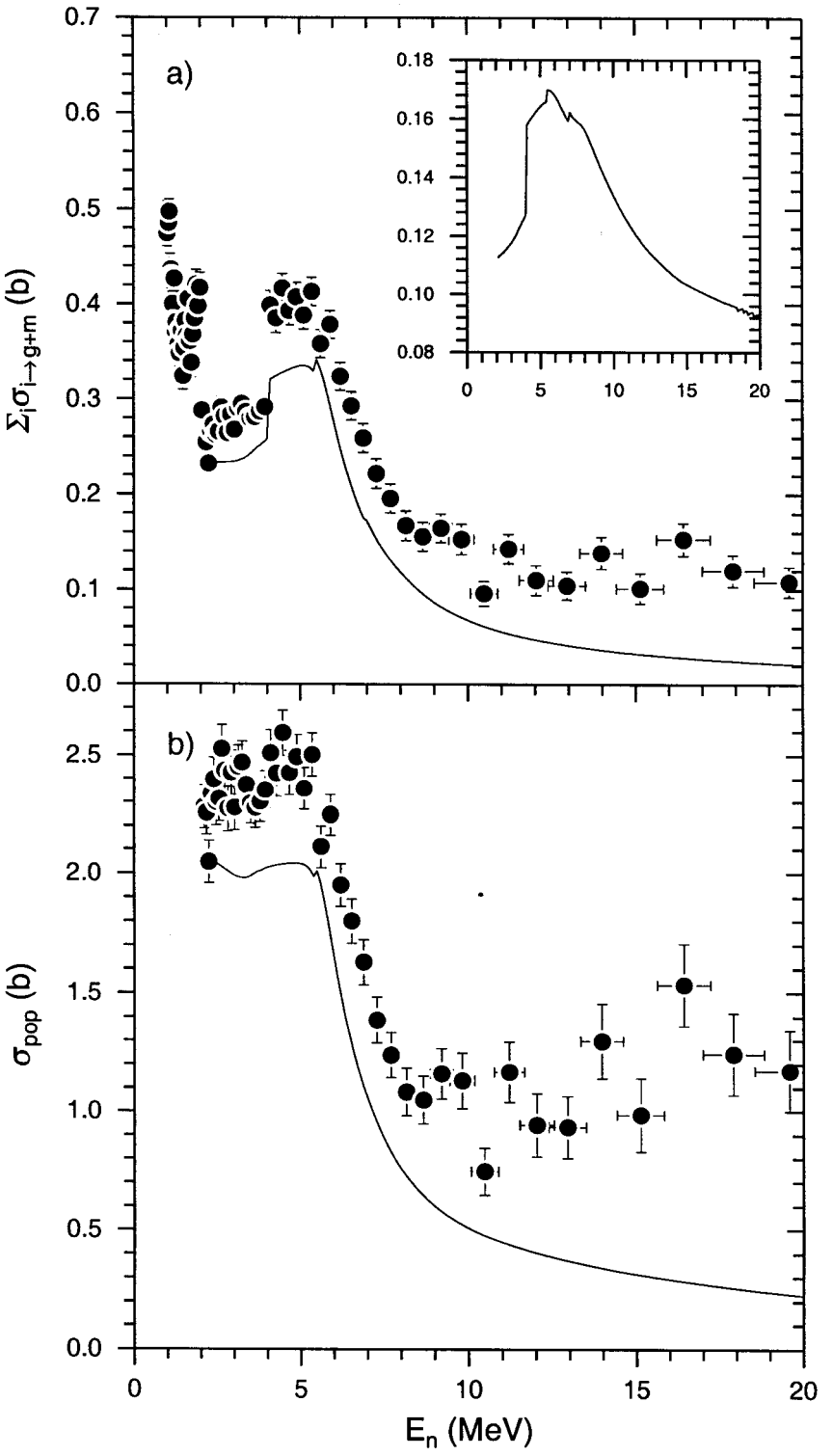


FIG. 22: Total-population cross section (panel b), deduced from the sum of parallel-path ($\sum_i \sigma^{(meas)}_{i\to g+m}$ in table I) transition cross sections (panel a) using Eqs. 1 and 2. The solid curve shows the **GNASH98** prediction in each case. The inset in panel a) shows the partial-to-total ratio, calculated in **GNASH98**, and used to deduce the population cross section. The apparent discontinuities at $E_n$ = 2 and 4 MeV in the data in panel a) are due to the exclusion of $\gamma$ rays in the $E_\gamma$ = 590–640-keV range for $E_n$ = 2-4 MeV (see text).

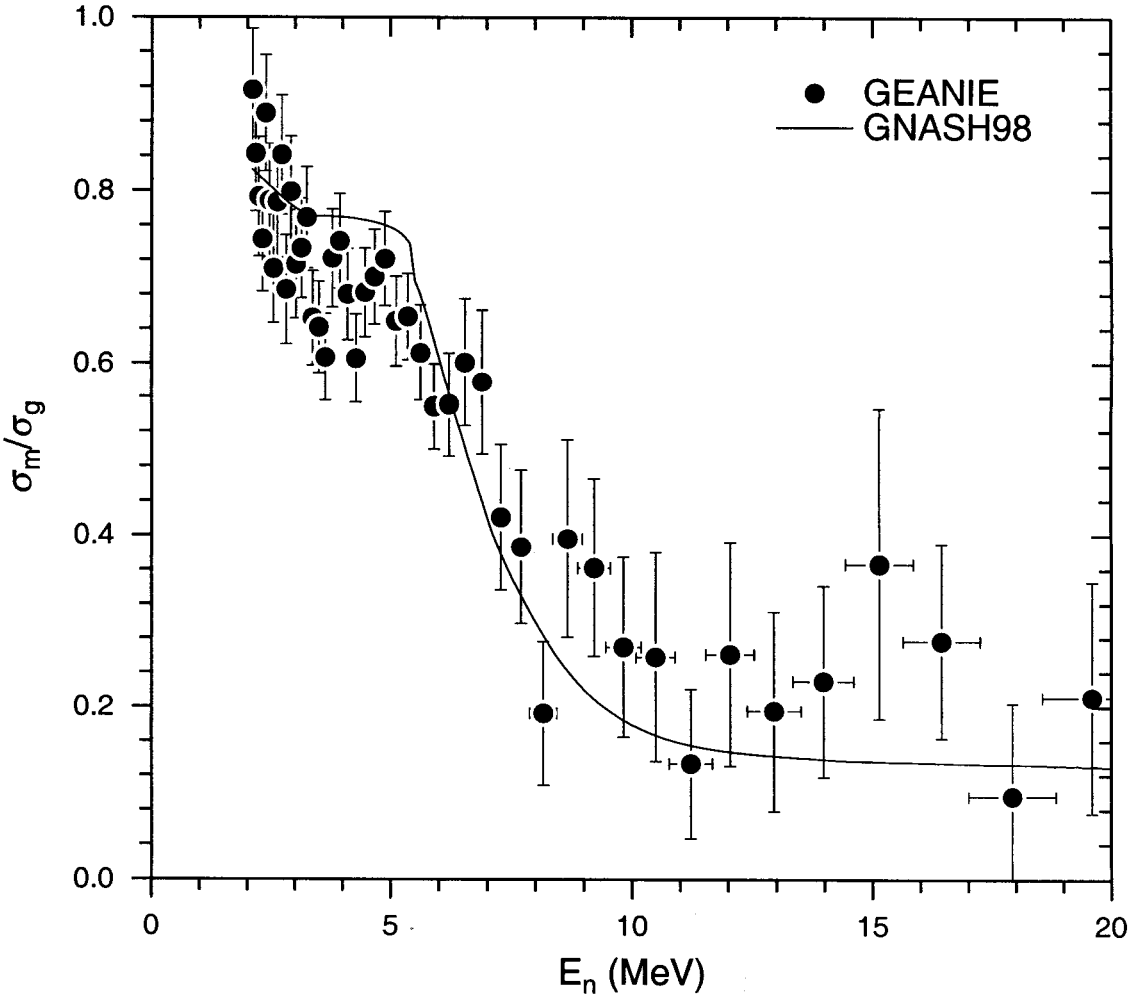


FIG. 23: Isomer-to-ground-state population ratio calculated using the deduced isomer-state and total population cross sections in Eq. A6.

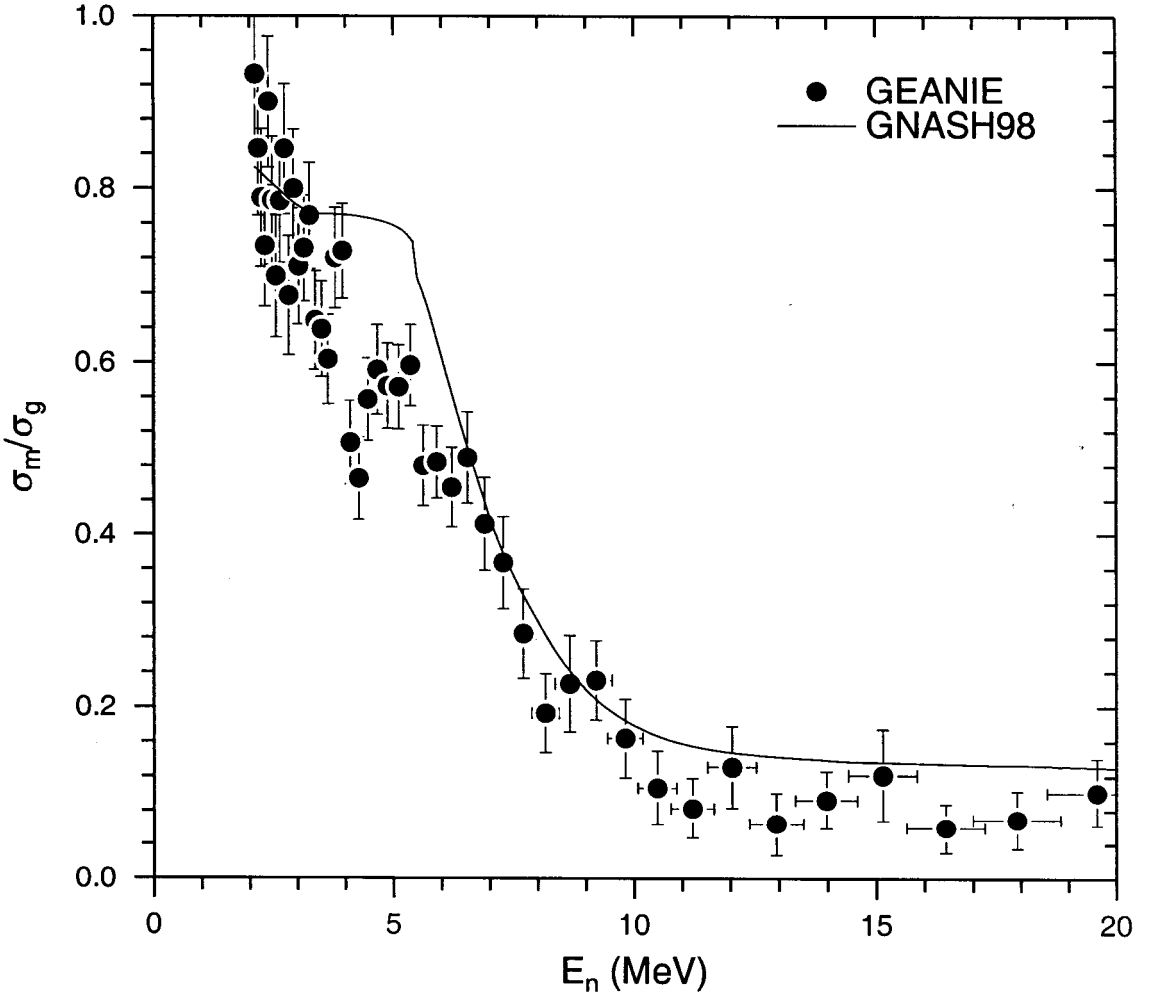


FIG. 24: Isomer-to-ground-state population ratio calculated using the deduced isomer- and ground-state population cross sections in Eq. A7. This approach produces smaller error bars than the prescription given in Eq. A6 and the resulting $\sigma_m/\sigma_g$ values are therefore preferred over those shown in Fig. 23.